J. Fluid Mech. (2013), *vol.* 726, *pp.* 439–475.
doi:10.1017/jfm.2013.210

The acoustic analogy in an annular duct with swirling mean flow

H. Posson† and N. Peake

Department of Applied Mathematics and Theoretical Physics, University of Cambridge, Wilberforce Road, Cambridge CB3 0WA, UK

(Received 9 August 2012; revised 18 February 2013; accepted 20 April 2013; first published online 10 June 2013)

This paper is concerned with modelling the effects of swirling flow on turbomachinery noise. We develop an acoustic analogy to predict sound generation in a swirling and sheared base flow in an annular duct, including the presence of moving solid surfaces to account for blade rows. In so doing we have extended a number of classical earlier results, including Ffowcs Williams & Hawkings' equation in a medium at rest with moving surfaces, and Lilley's equation for a sheared but non-swirling jet. By rearranging the Navier–Stokes equations we find a single equation, in the form of a sixth-order differential operator acting on the fluctuating pressure field on the left-hand side and a series of volume and surface source terms on the right-hand side; the form of these source terms depends strongly on the presence of swirl and radial shear. The integral form of this equation is then derived, using the Green's function tailored to the base flow in the (rigid) duct. As is often the case in duct acoustics, it is then convenient to move into temporal, axial and azimuthal Fourier space, where the Green's function is computed numerically. This formulation can then be applied to a number of turbomachinery noise sources. For definiteness here we consider the noise produced downstream when a steady distortion flow is incident on the fan from upstream, and compare our results with those obtained using a simplistic but commonly used Doppler correction method. We show that in all but the simplest case the full inclusion of swirl within an acoustic analogy, as described in this paper, is required.

Key words: acoustics, aeroacoustics

1. Introduction

Prediction and control of turbomachinery noise is a key challenge facing manufacturers of civil aeroengines. Strong swirling flow between rotor and stator stages is present throughout the engine, and is known to have a very significant effect on noise generation and propagation. The presence of swirl, however, introduces considerable theoretical complexity and is a subject of much current research (see Peake & Parry 2012). This paper considers the aeroacoustics of swirling mean flow in an annular duct. The first analysis of the effect of swirling mean flow on the properties of small disturbances in a duct is attributed to Kerrebrock (1977), who emphasized that the centrifugal and Coriolis forces produced by the mean swirl induce

† Email address for correspondence: helene.posson@gmail.com

a force imbalance that couples the vortical, entropic and acoustic disturbances, and deflects the fluid. Kerrebrock used a spectral method to analyse the propagation of small disturbances in an isentropic mean flow made up of a solid-body and a free-vortex swirl of small amplitude, and found 'shear' perturbations that are no longer purely convected, and may be associated with a weak pressure field. Further analysis of Kerrebrock's model has been performed by Roger & Arbey (1985). More recently, Kousen (1995, 1996) and Golubev & Atassi (1995, 1996, 1998) extended the result of Kerrebrock (1977) by removing the hypothesis of small swirling mean flow amplitude. In the presence of swirl, the modal disturbances split into two parts, the sonic modes and the nearly convected modes. The sonic modes, which are analogous to acoustic modes in irrotational flow, are pressure-dominated and are mostly sustained by compressibility effects. In addition to these sonic modes, the problem may involve other modes, the nearly convected modes, which are vorticity-dominated and are sustained by the mean vorticity. Finally, the singularity of the system of equations for the perturbations leads to the existence of a critical layer. As in irrotational flow, only a finite number of the sonic modes are propagating at any given frequency. On the contrary, there are often infinitely many nearly convected modes, which cluster at the ends of the critical layer. Tam & Auriault (1998) studied this problem for a non-homentropic swirling mean with uniform mean density, and also found the two families of sonic and nearly convected modes. In their study, the additional unstable mode observed is related to the mean flow, which is unstable in their case, as mentioned by Heaton & Peake (2006). Further, the spectrum with swirl has been investigated numerically with a finite element method by Nijboer (2001) for a homentropic flow, again exhibiting the two families of modes and the continuous spectrum of convected perturbations. The physical existence of the critical layer, or otherwise, has been debated in the literature. Heaton & Peake (2006) showed that a critical layer is present and corresponds to a continuous spectrum of perfectly convected perturbations. In addition, under some conditions, the continuous spectrum contribution can be unstable and grow algebraically downstream.

The presence of a swirling mean flow between the rotor and the stator of a fan stage significantly modifies both the vortical disturbances, such as the rotor wakes, as they evolve downstream, and the radiation of noise by the stator or the rotor. It is therefore important to account for swirl when predicting turbomachinery noise. Elhadidi *et al.* (2000) and Golubev & Atassi (2000*a*) predicted the downstream evolution of an incident vortical perturbation from the exit of the rotor by using an initial-value analysis, and pointed out how a change in the radial distribution of the swirl may lead to very different distortions of the wakes. The effect of the swirl on the rotor wakes has also been observed experimentally by Podboy *et al.* (2002*b*), for instance. Taking advantage of the large number of rotor blades, Cooper & Peake (2005) performed an asymptotic analysis to simplify the initial-value analysis. Then, a boundary layer correction had to be introduced to account for the impermeability of the duct walls. They observed the skewing of the wakes and the generation of a radial velocity component. Recently, Lloyd & Peake (2008) extended this work to include dissipative effects.

As emphasized by Atassi *et al.* (2004) and Cooper & Peake (2005), for instance, the swirling mean flow also significantly modifies the propagation of sonic modes (cut-on frequencies, radial distribution, existence of caustics, etc.). Golubev & Atassi (2000*b*) developed a model for the interaction of unsteady disturbances in a swirling mean flow with an annular cascade of unloaded blades using a linearized Euler code. The coupling between the potential and vortical parts of the unsteady velocity in

mean swirling flow is shown to be weak in a fan stage because of the large number of blades B (high associated reduced frequency), which allowed them to perform an asymptotic analysis. Ali & Atassi (2002), Elhadidi & Atassi (2002, 2003) and Atassi *et al.* (2004) extended this work, and found a strong dependence of the loading and the radiated noise on the swirl, and they confirmed the need to account for the effect of swirling mean flow when predicting rotor–stator interaction noise. Cooper & Peake (2005) developed an analytically based model to predict the rotor–stator interaction noise radiated upstream of the stator with swirl. Their large-B asymptotic analysis allows the evolving wake to be used as input into a local linear cascade of thick aerofoils, using the model of Evers & Peake (2002), with a mode matching strategy allowing the cascade radiation to be matched onto swirling duct modes. This demonstrates the strong effect of the radial distribution of the wake hitting the stator on the noise generation. This result was extended by Cooper & Peake (2006) to include various stator design features, such as lean and sweep.

We also note that the aeroacoustics of swirling flow has been studied in a number of other situations. Swirling jets have received much attention: see the experimental studies by Lu, Ramsay & Miller (1976) and by Yu & Chen (1997); while Carpenter (1985) develops a corresponding linear theory; and Cooper & Peake (2002) study the stability of a slowly spreading subsonic swirling jet. For internal flows, we mention here the experimental investigation of oscillatory instability in the so-called vortex whistle by Chanaud (1965). Howe & Liu (1977) derive a model for the sound generated when vorticity passes through a contraction in swirling ducted flow, while Carpenter & Johannesen (1975) extend classical theory to predict choking conditions for swirling flow.

Lighthill (1952) introduced his famous acoustic analogy to predict the noise of a turbulent jet by rearranging the Navier–Stokes equations for mass and momentum into a single equation for the fluctuating density with, on the left-hand side, the wave operator in an ambient medium at rest, and, on the right-hand side, all the remaining terms. The right-hand side is interpreted as an equivalent sound source, and can be written as the double divergence of the so-called Lighthill stress tensor T_{ij}. Lighthill's acoustic analogy can be extended to account for the presence of surfaces and to account for some propagation effects in a moving medium. We will discuss these two extensions briefly below, but see Colonius & Lele (2004) for a very detailed review.

First, Curle (1955) extended Lighthill's (1952) theory to account for the presence of static surfaces, using the Kirchhoff boundary solution to the homogeneous wave equation. He showed that the effects of the solid boundary are equivalent to a distribution of dipole sources representing the force per unit surface area acting on the fluid. Ffowcs Williams & Hawkings (1969) extended this further to account for the presence of arbitrary moving impermeable or permeable surfaces, by using generalized functions. In addition to sources corresponding to the surface force distributions, a surface term representing volume displacement effects now also appears. The Green's function in free space is often used to solve this equation, but Green's functions that are tailored to the geometry features can also be chosen.

Second, Lighthill's acoustic analogy may be extended to account for some propagation effects in a moving medium (convection, refraction, etc.), which gives the corresponding propagation operator on the left-hand side and a new source term on the right-hand side. In two different contexts (ducted flow and jets, respectively), Goldstein (1976) and Dowling, Ffowcs Williams & Goldstein (1978) introduced the effect of the convection of the waves by a uniform axial flow, which exhibits the convected wave operator on the left-hand side and the double divergence of a modified

Lighthill tensor (written for relative velocities) on the right-hand side. Famously, Lilley (1974) derived an acoustic analogy in a transverse shear flow, with, on the left-hand side, a third-order nonlinear operator acting on just the logarithm of the pressure – see the reviews of Doak (1972, 1973) for more details. This operator is often approximated by the (linear) Pridmore–Brown operator, and the right-hand side is often simplified, as given by Goldstein (1984). More recently, Colonius, Lele & Moin (1997) gave the exact source terms on the right-hand side of Lilley's equation, and Goldstein (2001) rearranged the Navier–Stokes equations as a single exact equation, with the Pridmore–Brown operator applied to new dependent variables to represent the pressure fluctuations on the left-hand side, and on the right-hand side the equivalent noise sources, which split into a quadrupole term and a dipole source produced by the temperature fluctuations. Morfey & Wright (2007) proposed a modified formulation of Ffowcs Williams & Hawkings' (1969) acoustic analogy that is more suitable for heated and inhomogeneous fluid flows. The density variable is replaced by either the pressure or a pressure-related variable to remove the local density from the source terms. Moreover, it can deal with initial-value problems by introducing equivalent new source terms.

In a slightly different direction, Goldstein (2003) developed a generalized acoustic analogy by recasting the full Navier–Stokes equation into a set of five linearized inhomogeneous Euler equations in convective form, for any chosen base flow and with different nonlinear dependent variables. Goldstein has also extended this formulation to include the presence of surfaces (M. E. Goldstein, private communication, 2012). The radiated field is obtained by using the vector Green's function associated with the linearized operator. Goldstein & Leib (2008) later used this approach to predict the sound from a unheated weakly non-parallel supersonic jet.

The present study aims at addressing the effect of swirling mean flow in turbomachinery noise. The approach adopted here is to develop an acoustic analogy similar to that of Lilley (1974) in sheared mean flow and to that of Goldstein (1976) in ducted uniform mean flow, but valid in the presence of sheared and swirling mean flow and of solid boundaries. It can be seen as a generalization of Ffowcs Williams & Hawkings' (1969) acoustic analogy to swirling mean flow with duct walls. First, the Navier–Stokes equations are written as linearized inhomogeneous Euler equations in cylindrical coordinates in § 2, and Ffowcs Williams & Hawkings' (1969) procedure is used to exhibit the equivalent volume and surface terms in §§ 3.1 and 3.2. Second, in § 3.3 this system of equations is recast to obtain, for the first time, a single sixth-order differential operator in time and space acting only on the fluctuating pressure field p on the left-hand side and a source term on the right-hand side. Third, in § 4 the Green's function tailored to the rigid annular duct with swirl is derived in the frequency domain. Fourth, the formulation to be used in the fan noise context is detailed in § 5. This formulation can be applied to a range of tonal and broadband fan noise sources, including rotor-alone trailing-edge noise and rotor–stator interaction noise, which will be the subject of further publication. However, as the first application of our new theory, the noise produced by the interaction of an incoming steady non-uniform flow with the fan (so-called fan inflow distortion tone noise) is investigated in § 6 to emphasize the possible effects of swirling mean flow for a less complicated noise mechanism. For swirl distributions that are most representative of the industrial situation, we will show that full consideration of the swirl, as presented in this paper, is required.

2. Navier–Stokes equations: linearized inhomogeneous Euler equations

Let us consider an infinite cylindrical annulus, $h \leqslant r \leqslant 1$, with hard impermeable walls at $r = h$ and $r = 1$, where r, θ, x are non-dimensional cylindrical polar coordinates. Throughout, dimensional variables are marked with an asterisk, and results are given in a non-dimensional form, where lengths are made non-dimensional by the outer radius of the duct, R_T^*, densities by the mean flow density at $r = 1$, $\rho_0^*(R_T^*)$, and velocities by the mean sound speed at $r = 1$, $c_0^*(R_T^*)$. Let $\boldsymbol{u}_{to} = (u_{to}, v_{to}, w_{to})$, ρ_{to} and p_{to} be the total variables (velocity, density and pressure) of the compressible flow. The base flow is chosen to be representative of a swirling mean flow between the rotor and the stator, neglecting viscous and dissipation effects (but note that we will include dissipation in the unsteady flow). It is defined as subsonic, inviscid and homentropic, with velocity

$$\boldsymbol{U} = (U_r, U_\theta, U_x) = (0, U_\theta(r), U_x(r)), \tag{2.1}$$

density $\rho_0(r)$ and pressure $P_0(r)$, and satisfies $\mathrm{d}P_0/\mathrm{d}r = \rho_0 U_\theta^2/r$, with

$$c_0^2(r) = c_0^2(1) + (\gamma - 1)\int_1^r \frac{U_\theta(r')^2}{r'}\,\mathrm{d}r'. \tag{2.2}$$

Let $\boldsymbol{u} = (u, v, w)$, ρ and p be the associated perturbations to this base flow, that is to say,

$$\boldsymbol{u}_{to} = \boldsymbol{U} + \boldsymbol{u}, \quad \rho_{to} = \rho_0 + \rho, \quad p_{to} = P_0 + p. \tag{2.3}$$

The compressible Navier–Stokes equations in cylindrical coordinates can be exactly rearranged as a linear operator acting on the perturbations on the left-hand side with a right-hand side including all nonlinear, viscous and non-isentropic effects:

$$\frac{1}{c_0^2}\frac{\mathrm{D}_0 p}{\mathrm{D}t} + u\frac{\mathrm{d}\rho_0}{\mathrm{d}r} + \rho_0 \operatorname{div}\boldsymbol{u} = S_\rho, \tag{2.4}$$

$$\rho_0\left[\frac{\mathrm{D}_0 v}{\mathrm{D}t} + \frac{u}{r}\frac{\mathrm{d}(rU_\theta)}{\mathrm{d}r}\right] + \frac{1}{r}\frac{\partial p}{\partial \theta} = S_\theta, \tag{2.5}$$

$$\rho_0\left[\frac{\mathrm{D}_0 u}{\mathrm{D}t} - 2\frac{U_\theta}{r}v\right] + \frac{\partial p}{\partial r} - \frac{U_\theta^2}{rc_0^2}p = S_r, \tag{2.6}$$

$$\rho_0\left[\frac{\mathrm{D}_0 w}{\mathrm{D}t} + u\frac{\mathrm{d}U_x}{\mathrm{d}r}\right] + \frac{\partial p}{\partial x} = S_x, \tag{2.7}$$

together with the energy equation (not given here), where the operator

$$\frac{\mathrm{D}_0}{\mathrm{D}t} = \frac{\partial}{\partial t} + U_x\frac{\partial}{\partial x} + U_\theta\frac{\partial}{r\,\partial\theta} \tag{2.8}$$

is the convective derivative linearized around the base flow and t is the time,

$$S_\rho = -\operatorname{div}(\rho\boldsymbol{u}) + \frac{\mathrm{D}_0 Z}{\mathrm{D}t}, \tag{2.9}$$

where the non-isentropic factor Z is

$$Z = (p - c_0^2\rho)/c_0^2, \tag{2.10}$$

and the vector $\boldsymbol{S} = (S_r, S_\theta, S_x)$ is defined by

$$\boldsymbol{S} = \boldsymbol{\nabla}\cdot\overline{\overline{\boldsymbol{\tau}}}_{to} - \rho_{to}(\boldsymbol{u}\cdot\boldsymbol{\nabla})\boldsymbol{u} - \rho\frac{\mathrm{D}_0\boldsymbol{u}}{\mathrm{D}t_0} - \rho\mathcal{H} - \frac{U_\theta^2}{r_0}Z\boldsymbol{e_r}, \tag{2.11}$$

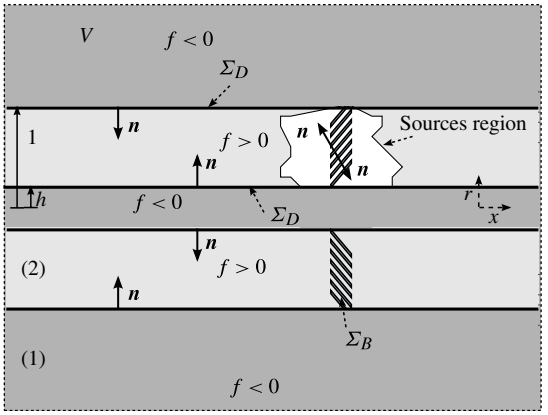

FIGURE 1. Sketch of the problem and the notation.

where $\overline{\overline{\boldsymbol{\tau}}}_{to}$ is the viscous stress tensor and

$$\mathcal{H} = -2\frac{U_\theta}{r} v\, \boldsymbol{e_r} + \frac{u}{r}\frac{\mathrm{d}(rU_\theta)}{\mathrm{d}r}\, \boldsymbol{e_\theta} + \frac{\mathrm{d}U_x}{\mathrm{d}r} u\, \boldsymbol{e_x}. \tag{2.12}$$

This system of equations will be referred to later as

$$\mathscr{L}(\boldsymbol{u}, \rho, p) = \begin{pmatrix} S_\rho \\ \boldsymbol{S} \end{pmatrix}. \tag{2.13}$$

3. Derivation of the governing equation for the pressure field in an annular duct with swirling mean flow

The approach proposed by Ffowcs Williams & Hawkings (1969) generalizes Lighthill's (1952) acoustic analogy to include the presence of (possibly moving) surfaces and uses the free-space Green's function for a medium at rest. The purpose of this section is to apply the approach developed by Ffowcs Williams & Hawkings (1969) to the present configuration involving duct walls and a swirling mean flow.

3.1. *Definitions of the surface and of the generalized functions*

Let $\Sigma(t)$ be the set of the B blade surfaces $\Sigma_B = \bigcup_{j=0:B-1} \Sigma_{B,j}$ and of the hub and tip duct surfaces $\Sigma_D = \Sigma_{hub} \cup \Sigma_{tip}$, so that $\Sigma = \Sigma_B \cup \Sigma_D$. The surface Σ can be defined by

$$\begin{cases} f(\boldsymbol{x}, t) = 0 & \text{on } \Sigma(t), \\ f(\boldsymbol{x}, t) > 0 & \text{in the fluid, volume } \mathscr{V}(t), \\ f(\boldsymbol{x}, t) < 0 & \text{outside } \mathscr{V}(t). \end{cases} \tag{3.1}$$

A sketch of the problem is shown in figure 1. The fluid region outside Σ is referred to as region (2), and the region inside the surface Σ is referred to as region (1); $\nabla f = \boldsymbol{n}$ is the outward unit normal of the surface Σ directed into the fluid, i.e. from region (1) to region (2). Let us define $\boldsymbol{v}^\Sigma$ to be the surface speed. For any variable φ defined in the fluid domain $\mathscr{V}(t)$, it is possible to define the generalized function $\widetilde{\varphi}$ in the whole space, and equal to φ inside the fluid and zero outside, by $\widetilde{\varphi} = H(f)\,\varphi$. In the following, the tilde symbol denotes generalized functions and generalized derivatives.

3.2. *Linearized inhomogeneous Euler equations in the sense of generalized functions*

Let us multiply (2.4)–(2.7) by $H(f)$ and use the three relations $\partial f/\partial t = -\boldsymbol{v}^{\Sigma}\cdot\boldsymbol{n}$, $\boldsymbol{\nabla}[H(f)] = \delta(f)\boldsymbol{n}$ and $\partial[H(f)]/\partial t = -\boldsymbol{v}^{\Sigma}\cdot\boldsymbol{n}\,\delta(f)$ (see e.g. Farassat 1977, 1994; Jones 1982). Then, the system of equations (2.13) becomes

$$\widetilde{\mathscr{L}}(\widetilde{\boldsymbol{u}},\widetilde{\rho},\widetilde{p}) = \begin{pmatrix}\widetilde{S}_{\rho}\\ \widetilde{\boldsymbol{S}}\end{pmatrix} + \begin{pmatrix}S_{FWH,\rho}\\ \boldsymbol{S}_{FWH}\end{pmatrix}\delta(f), \tag{3.2}$$

where the operator $\widetilde{\mathscr{L}}$ is the generalized operator $\mathscr{L}$, $\widetilde{S}_{\rho}$ and $\widetilde{\boldsymbol{S}}$ stand for the generalized source terms given by replacing the physical variables in (2.9) and (2.11) by the generalized variables, and $S_{FWH,\rho}\delta(f)$ and $\boldsymbol{S}_{FWH}\delta(f)$ are additional surface source terms arising from the use of the generalized function and the presence of the surface Σ. They are defined by

$$\begin{aligned}\boldsymbol{S}_{FWH} &= (S_{FWH,r}, S_{FWH,\theta}, S_{FWH,x}) = \overline{\overline{\boldsymbol{L}}}\cdot\boldsymbol{n}\\ &= \rho_{to}\boldsymbol{u}(\boldsymbol{u}+\boldsymbol{U}-\boldsymbol{V}^{\Sigma})\cdot\boldsymbol{n} + p\boldsymbol{n} - \overline{\overline{\boldsymbol{\tau}}}_{to}\cdot\boldsymbol{n}\\ &= \rho_{to}\boldsymbol{u}(\boldsymbol{u}_{to}-\boldsymbol{V}^{\Sigma})\cdot\boldsymbol{n} + p\boldsymbol{n} - \overline{\overline{\boldsymbol{\tau}}}_{to}\cdot\boldsymbol{n},\end{aligned} \tag{3.3}$$

which will later be related to the loading noise, and

$$\begin{aligned}S_{FWH,\rho} &= \rho_{to}(\boldsymbol{u}+\boldsymbol{U}-\boldsymbol{V}^{\Sigma})\cdot\boldsymbol{n} - \rho_0(\boldsymbol{U}-\boldsymbol{V}^{\Sigma})\cdot\boldsymbol{n} = \boldsymbol{Q}\cdot\boldsymbol{n}\\ &= \rho_{to}(\boldsymbol{u}_{to}-\boldsymbol{V}^{\Sigma})\cdot\boldsymbol{n} - \rho_0(\boldsymbol{U}-\boldsymbol{V}^{\Sigma})\cdot\boldsymbol{n},\end{aligned} \tag{3.4}$$

which will later be related to the thickness noise (e.g. Goldstein 1976; Hanson 1976). Since there are zero fluctuations in region (1), surface terms $[\boldsymbol{S}_{FWH}]_1^2\delta(f)$ and $[S_{FWH,\rho}]_1^2\delta(f)$ are simply evaluated from the value on the surface in the fluid region (2), and the index (2) is omitted in the following expressions. The two surface terms (3.3) and (3.4) generalize the surface source terms obtained by Ffowcs Williams & Hawkings (1969) in a medium at rest and the surface source terms given by Najafi-Yazdi, Brès & Mongeau (2011) in the case of an axial uniform mean flow, to a more general medium with sheared and/or swirling mean flow. Our expressions are very similar to these previous results, but there are two differences. First, the definition of $\boldsymbol{u}$ differs. It is equal to $\boldsymbol{u}_{to}$ in zero base flow (medium at rest), to $\boldsymbol{u}_{to} - U_x\boldsymbol{e}_x$ in a uniform axial base flow and to $\boldsymbol{u}_{to} - U_x(r)\boldsymbol{e}_x - U_{\theta}(r)\boldsymbol{e}_{\theta}$ in the present case. This modifies the velocity $\boldsymbol{u}$ in front of the brackets in the first term of (3.3) and the base flow velocity $\boldsymbol{U}$ in the second term of (3.4). Second, we allow the base flow pressure P_0 and density ρ_0 to vary spatially (along the radial direction). Finally, some specific configurations may occur. If the surface Σ is rigid, i.e. impermeable and non-vibrating, $(\boldsymbol{U}+\boldsymbol{u})\cdot\boldsymbol{n} = \boldsymbol{V}^{\Sigma}\cdot\boldsymbol{n}$, and the first terms in (3.3) and (3.4) are zero. If the base flow is parallel to the surfaces (for instance, if there is no angle of attack on the blades), $\boldsymbol{U}\cdot\boldsymbol{n} = \boldsymbol{V}^{\Sigma}\cdot\boldsymbol{n}$, and the second term in (3.4) is zero.

3.3. *Sixth-order partial differential equation for the fluctuating pressure field*

Goldstein (1976, chap. 4) derived an acoustic analogy for a uniform mean flow confined in a circular duct, a result that is easily transposed to an annular cross-section using the proper eigenfunctions and the associated tailored Green's function. This acoustic analogy is often used to predict the rotor–stator interaction tonal noise (as proposed by Ventres, Theobald & Mark (1982)), or even the rotor–stator interaction broadband noise (again as proposed by Ventres *et al.* (1982) and used by Nallasamy & Envia (2005) or Posson, Moreau & Roger (2011)), or the rotor

self-noise (as investigated by Glegg & Jochault 1998). Like the acoustic analogies of Lighthill (1952) and Ffowcs Williams & Hawkings (1969), this acoustic analogy relies on solving one single inhomogeneous second-order partial differential equation for the fluctuating density (or pressure). The left-hand side is seen as a wave operator and the right-hand side is an equivalent source. The pressure field can be expressed by introducing a scalar Green's function associated with the left-hand side operator, and tailored to the rigid boundary conditions of the duct walls. The pressure field is given in terms of a volume integral, which is interpreted as a volume quadrupole source term, and two surface source terms, referred to as the thickness or volume displacement term and the loading noise term. In practice, in the subsonic regime, the volume term and the surface term corresponding to the volume displacement effect are often neglected.

Our present result, written as a system of four equations in (3.2), could be used as it is to solve for the pressure, and to do this it would require us to introduce a vector Green's function, as proposed by Goldstein (2003) in another context (here with the surface terms). However, it is attractive to be able to write the problem in terms of a single scalar equation for the pressure field. First, it will allow the swirling problem to be written in exactly the same form as has been done for uniform and sheared axial mean flows, and therefore allow direct comparison between the various cases. Second, it may be more efficient to solve numerically a single equation. In particular, when working in the frequency domain and Fourier space, the system may be reduced to a low-order ordinary differential equation (ODE) in the radial direction.

After some considerable algebra, described in appendix A, the problem reduces to a single equation with a sixth-order operator $\mathscr{F}$ in time and space operating on only the fluctuating pressure field p on the left-hand side and a source term on the right-hand side:

$$\mathscr{F}(p) = \widetilde{\mathbb{S}} + \mathbb{S}_{FWH}, \tag{3.5}$$

with

$$\begin{aligned}\mathscr{F}(p) = \mathscr{D}\left(\frac{\mathrm{D}_0}{\mathrm{D}t}\left(\frac{\partial}{\partial r}\left(\mathscr{M}(p)\right)\right)\right) + \left\{\left[\frac{1}{r}\frac{\mathrm{D}_0}{\mathrm{D}t} - \frac{\mathrm{d}(rU_\theta)}{r\,\mathrm{d}r}\frac{\partial}{r\,\partial\theta} - \frac{\mathrm{d}U_x}{\mathrm{d}r}\frac{\partial}{\partial x}\right]\mathscr{D}\right.\\ \left. + 2\frac{\mathrm{D}_0^2}{\mathrm{D}t^2}\left[\frac{\mathrm{d}U_x}{\mathrm{d}r}\frac{\partial}{\partial x} + \frac{\mathrm{d}}{\mathrm{d}r}\left(\frac{U_\theta}{r}\right)\frac{\partial}{\partial\theta}\right] + \frac{\mathrm{d}}{\mathrm{d}r}\left[\frac{2U_\theta}{r^2}\frac{\mathrm{d}(rU_\theta)}{\mathrm{d}r}\right]\frac{\mathrm{D}_0}{\mathrm{D}t}\right\}\mathscr{M}(p)\\ - \left[\frac{\partial^2}{r^2\,\partial\theta^2} + \frac{\partial^2}{\partial x^2} - \frac{1}{c_0^2}\frac{\mathrm{D}_0^2}{\mathrm{D}t^2}\right]\mathscr{D}^2(p)\end{aligned} \tag{3.6}$$

and

$$\widetilde{\mathbb{S}} = \mathscr{A}(\widetilde{\mathbb{S}}_1) + \mathscr{D}^2(\widetilde{\mathbb{S}}_2) \quad \text{and} \quad \mathbb{S}_{FWH} = \mathscr{A}(\mathbb{S}_{FWH,1}) + \mathscr{D}^2(\mathbb{S}_{FWH,2}), \tag{3.7}$$

where the operator $\mathscr{A}$ is

$$\begin{aligned}\mathscr{A}(\varphi) = \left\{\mathscr{D}\left[\frac{\mathrm{D}_0}{\mathrm{D}t}\left(\frac{1}{r} + \frac{\partial}{\partial r}\right) - \frac{\mathrm{d}(rU_\theta)}{r\,\mathrm{d}r}\frac{\partial}{r\,\partial\theta} - \frac{\mathrm{d}U_x}{\mathrm{d}r}\frac{\partial}{\partial x}\right]\right.\\ \left. + 2\frac{\mathrm{D}_0^2}{\mathrm{D}t^2}\left[\frac{\mathrm{d}U_x}{\mathrm{d}r}\frac{\partial}{\partial x} + \frac{\mathrm{d}}{\mathrm{d}r}\left(\frac{U_\theta}{r}\right)\frac{\partial}{\partial\theta}\right] + \frac{\mathrm{d}}{\mathrm{d}r}\left[\frac{2U_\theta}{r^2}\frac{\mathrm{d}(rU_\theta)}{\mathrm{d}r}\right]\frac{\mathrm{D}_0}{\mathrm{D}t}\right\}(\varphi)\end{aligned} \tag{3.8}$$

and the source terms are

$$\widetilde{\mathbb{S}}_1 = \frac{\mathrm{D}_0\widetilde{S}_r}{\mathrm{D}t} + 2\frac{U_\theta}{r}\widetilde{S}_\theta, \quad \widetilde{\mathbb{S}}_2 = \frac{\mathrm{D}_0\widetilde{S}_\rho}{\mathrm{D}t} - \frac{1}{r}\frac{\partial\widetilde{S}_\theta}{\partial\theta} - \frac{\partial\widetilde{S}_x}{\partial x}, \tag{3.9}$$

and

$$\mathbb{S}_{FWH,1} = \frac{\mathrm{D}_0[S_{FWH,r}\delta(f)]}{\mathrm{D}t} + 2\frac{U_\theta}{r}S_{FWH,\theta}\delta(f), \tag{3.10a}$$

$$\mathbb{S}_{FWH,2} = \frac{\mathrm{D}_0[S_{FWH,\rho}\delta(f)]}{\mathrm{D}t} - \frac{1}{r}\frac{\partial[S_{FWH,\theta}\delta(f)]}{\partial\theta} - \frac{\partial[S_{FWH,x}\delta(f)]}{\partial x}. \tag{3.10b}$$

Equation (3.5) is the key result of this paper, and will be applied to the prediction of turbomachinery noise in later sections.

It is worth checking that, in the particular case of a fluid with no swirl ($U_\theta = 0$) and no solid surfaces, Lilley's (1974) equation restricted to an isentropic shear flow is recovered from (3.5). In this case, the fluid occupies the whole space, i.e. $f > 0$ and $\widetilde{\varphi} = \varphi$ everywhere, $\mathrm{D}_0/\mathrm{D}t = \partial/\partial t + U_x\,\partial/\partial x$ and $\mathscr{D} = -\mathrm{D}_0^2/\mathrm{D}t^2$. Replacing these expressions in the sixth-order operator defined by (3.6) leads to

$$\mathscr{F}(p) = \frac{\mathrm{D}_0^3}{\mathrm{D}t^3}\left[\frac{\mathrm{D}_0}{\mathrm{D}t}\left(\frac{1}{c_0^2}\frac{\mathrm{D}_0^2 p}{\mathrm{D}t^2} - \nabla^2 p\right) + 2\frac{\mathrm{d}U_1}{\mathrm{d}y_2}\frac{\partial^2 p}{\partial y_1\,\partial y_2}\right], \tag{3.11}$$

where now, in order to match with Lilley's (1974) original notation, we take the 1 and 2 directions to be aligned with the x axis and the direction of radial shear, respectively. Let

$$T_{ij} = \rho_{to}u_i u_j + (p - c_0^2\rho)\delta_{ij} - \tau_{ij} = \rho_{to}u_i u_j - \tau_{ij} + c_0^2 Z\delta_{ij} \tag{3.12}$$

be the modified Lighthill tensor. It differs from Lighthill's (1952) tensor in the fact that u_i is now the fluctuating velocity component around the chosen base flow instead of the total velocity component in a medium at rest. Then, in the same way as above, and introducing the same assumptions as Goldstein (1976) and Goldstein (1984, §§ 6.5–6.6) (so that $Z = p/c_0^2 - \rho = 0$ and $\overline{\overline{\boldsymbol{\tau}}} = 0$), the source term becomes

$$\mathbb{S} = \frac{\mathrm{D}_0^3}{\mathrm{D}t^3}\left\{\frac{\mathrm{D}_0}{\mathrm{D}t}\left[\frac{\partial^2\rho_{to}\,u_i u_j}{\partial y_i\,\partial y_j}\right] - 2\frac{\mathrm{d}U_1}{\mathrm{d}y_2}\frac{\partial^2(\rho_{to}u_2 u_i)}{\partial y_1\,\partial y_i}\right\}. \tag{3.13}$$

Putting this together, we therefore find that the pressure field is the solution of

$$\begin{aligned}\frac{\mathrm{D}_0^3}{\mathrm{D}t^3}&\left\{\frac{\mathrm{D}_0}{\mathrm{D}t}\left(\frac{1}{c_0^2}\frac{\mathrm{D}_0^2 p}{\mathrm{D}t^2} - \nabla^2 p\right) + 2\frac{\mathrm{d}U_1}{\mathrm{d}y_2}\frac{\partial^2 p}{\partial y_1\,\partial y_2}\right\}\\ &= \frac{\mathrm{D}_0^3}{\mathrm{D}t^3}\left\{\frac{\mathrm{D}_0}{\mathrm{D}t}\left[\frac{\partial^2\rho_{to}\,u_i u_j}{\partial y_i\,\partial y_j}\right] - 2\frac{\mathrm{d}U_1}{\mathrm{d}y_2}\frac{\partial^2(\rho_{to}u_2 u_i)}{\partial y_1\,\partial y_i}\right\}.\end{aligned} \tag{3.14}$$

If the third-order convective derivative $\mathrm{D}_0^3/\mathrm{D}t^3$ is now removed from both sides, we find Lilley's (1974) equation. (But note that we have assumed here that the fluctuations are isentropic and that the fluctuating pressure is sufficiently small so that the operator $\Pi = \log(p/P_0)$ of Lilley can be approximated by $\Pi \approx p/(\gamma P_0) = p/(c_0^2\rho_0)$ – see e.g. Goldstein (1976, § 6), Goldstein (1984), Colonius *et al.* (1997) and Goldstein (2001).) It therefore follows that our new (3.5) reduces to the Lilley's (1974) well-known equation in the limit of zero swirl and in the absence of solid boundaries.

4. Green's function tailored to a rigid infinite annular duct with swirling mean flow

Before we can apply (3.5) to noise prediction in swirling flow, we must first compute the appropriate Green's function. Let G be the Green's function tailored to a

rigid infinite annular duct with swirling mean flow, namely G is the solution of

$$\mathscr{F}(G) = \delta(x - x_0)\frac{\delta(r - r_0)}{r_0}\sum_{n\in\mathbb{Z}}\delta(\theta - \theta_0 - 2\pi n)\delta(t - t_0), \tag{4.1}$$

together with the boundary condition that the normal velocity associated with G is zero on the duct walls. In (4.1), the sum over n simply enforces the 2π periodicity caused by the annular geometry (see e.g. Jones 1982, p. 304), and the $1/r_0$ comes from the Dirac delta function in the azimuthal direction. Notice that the convention of the positive right-hand side is chosen for consistency with the uniform mean flow case (Goldstein 1976; Ventres *et al.* 1982; Posson *et al.* 2011).

4.1. *Expression for the Green's function*

Let us introduce the Fourier transforms in time t and axial direction x, and the Fourier series in the azimuthal direction θ. Then G can be defined in terms of its Fourier components:

$$G(\boldsymbol{x}, t \,|\, \boldsymbol{x}_0, t_0) = \int\sum_{m\in\mathbb{Z}}\int \widehat{G}_m(r \,|\, k, \omega, \boldsymbol{x}_0, t_0)\,\mathrm{e}^{\mathrm{i}kx}\,\mathrm{d}k\,\mathrm{e}^{\mathrm{i}m\theta}\mathrm{e}^{-\mathrm{i}\omega t}\,\mathrm{d}\omega. \tag{4.2}$$

In the frequency domain, the inversion contours in the complex k–ω plane are chosen to give a causal solution by applying the Briggs–Bers (Briggs 1964; Bers 1983) procedure in a standard manner. By the linearity of the problem, let us consider one particular Fourier component $\widehat{G}_m(r \,|\, k, \omega, \boldsymbol{x}_0, t_0)$ for a triplet (k, m, ω). In Fourier space, (4.1) becomes

$$-D_{m,k}(r)^2\Lambda_{m,k}(r)^2\mathscr{L}_m(\widehat{G}_m) = \frac{\delta(r - r_0)}{(2\pi)^3 r_0}\,\mathrm{e}^{-\mathrm{i}kx_0 + \mathrm{i}\omega t_0 - \mathrm{i}m\theta_0}, \tag{4.3}$$

with

$$\mathscr{L}_m(\widehat{p}) = \frac{1}{r}\frac{\mathrm{d}}{\mathrm{d}r}\left(\frac{r}{D_{m,k}}\left(B_{m,k}\widehat{p} + \frac{\mathrm{d}\widehat{p}}{\mathrm{d}r}\right)\right) - \frac{2mU_\theta}{\Lambda_{m,k}r^2D_{m,k}}\left(B_{m,k}\widehat{p} + \frac{\mathrm{d}\widehat{p}}{\mathrm{d}r}\right) + \frac{1}{\Lambda_{m,k}^2}\left(\frac{\Lambda_{m,k}^2}{c_0^2} - \frac{m^2}{r^2} - k^2\right)\widehat{p}, \tag{4.4}$$

where

$$\Lambda_{m,k}(\omega) = kU_x + \frac{mU_\theta}{r} - \omega, \tag{4.5a}$$

$$D_{m,k}(\omega, r) = \Lambda_{m,k}^2(\omega) - \frac{2U_\theta}{r^2}\frac{\mathrm{d}(rU_\theta)}{\mathrm{d}r}, \tag{4.5b}$$

$$B_{m,k}(r) = \frac{2mU_\theta}{\Lambda_{m,k}r^2} - \frac{U_\theta^2}{rc_0^2}. \tag{4.5c}$$

Taking the Fourier transform in x and t and the Fourier series of (A 4), and setting the radial velocity component to zero gives the boundary condition

$$B_{m,k}\widehat{G}_m + \frac{\partial\widehat{G}_m}{\partial r} = 0 \quad \text{at } r = h \text{ and } r = 1. \tag{4.6}$$

With no swirl ($U_\theta = 0$), $B_{m,k} = 0$, and the boundary condition of rigid duct walls is equivalent to a zero normal pressure gradient, as obtained with uniform mean flow.

Equivalently $\widehat{G}_m$ is defined by

$$\widehat{G}_m(r\,|\,k,\omega,\boldsymbol{x}_0,t_0)=\widehat{\widehat{G}}_m(r\,|\,k,\omega,r_0)\,\mathrm{e}^{-\mathrm{i}kx_0+\mathrm{i}\omega t_0-\mathrm{i}m\theta_0}=\frac{\widehat{p}_{G,m}(r\,|\,k,\omega,\boldsymbol{x}_0,t_0)}{D_{m,k}(r_0)\Lambda_{m,k}(r_0)^2},\tag{4.7}$$

with $\widehat{p}_{G,m}$ the solution of

$$D_{m,k}\,\mathscr{L}_m(\widehat{p}_{G,m})=-\frac{\delta(r-r_0)}{(2\pi)^3 r_0}\mathrm{e}^{-\mathrm{i}kx_0+\mathrm{i}\omega t_0-\mathrm{i}m\theta_0},\tag{4.8}$$

with

$$B_{m,k}\widehat{p}_{G,m}+\frac{\partial\widehat{p}_{G,m}}{\partial r}=0\quad\text{at } r=h \text{ and } r=1.\tag{4.9}$$

Equations (4.8) and (4.9) and their solution are very similar to the results given by Heaton & Peake (2006), but they differ because we consider here the pressure Green's function instead of the velocity potential Green's function, and because of our inclusion of the $1/r_0$ factor in the pulse source to deal with the pulse source in cylindrical coordinates.

The solution of (4.8) is continuous at $r=r_0$ but its derivative jumps (see e.g. Reinhard 1982),

$$\left[\frac{\partial\widehat{p}_{G,m}(r\,|\,k,\omega,\boldsymbol{x}_0,t_0)}{\partial r}\right]_{r=r_0^-}^{r=r_0^+}=-\frac{\mathrm{e}^{-\mathrm{i}kx_0+\mathrm{i}\omega t_0-\mathrm{i}m\theta_0}}{(2\pi)^3 r_0}.\tag{4.10}$$

Using the general theory of differential equations (see e.g. Bender & Orszag 1978), the Green's function $\widehat{p}_{G,m}$ is found to be

$$\widehat{p}_{G,m}(r\,|\,k,\omega,\boldsymbol{x}_0,t_0)=-\frac{\mathrm{e}^{-\mathrm{i}kx_0+\mathrm{i}\omega t_0-\mathrm{i}m\theta_0}}{(2\pi)^3 r_0 K(k,r_0)}\begin{cases}\widehat{p}_{G,m,2}(k,r_0)\widehat{p}_{G,m,1}(k,r), & r\leqslant r_0,\\ \widehat{p}_{G,m,1}(k,r_0)\widehat{p}_{G,m,2}(k,r), & r>r_0,\end{cases}\tag{4.11}$$

where $\widehat{p}_{G,m,1}$ and $\widehat{p}_{G,m,2}$ are two solutions of the homogeneous equation $\mathscr{L}_m(\widehat{p})=0$ satisfying the boundary conditions

$$\begin{cases}B_{m,k}(h)\widehat{p}_{G,m,1}(k,h)+\dfrac{\partial\widehat{p}_{G,m,1}}{\partial r}(k,h)=0,\\ h\widehat{p}_{G,m,1}(k,h)=1,\end{cases}\tag{4.12}$$

and

$$\begin{cases}\widehat{p}_{G,m,2}(k,1)=1,\\ B_{m,k}(1)\widehat{p}_{G,m,2}(k,1)+\dfrac{\partial\widehat{p}_{G,m,2}}{\partial r}(k,1)=0,\end{cases}\tag{4.13}$$

respectively, and where

$$K(k,r_0)=\widehat{p}_{G,m,1}(k,r_0)\frac{\partial\widehat{p}_{G,m,2}}{\partial r}(k,r_0)-\widehat{p}_{G,m,2}(k,r_0)\frac{\partial\widehat{p}_{G,m,1}}{\partial r}(k,r_0).\tag{4.14}$$

From Bender & Orszag (1978, chap. 1, Part I), it can be shown that

$$K(k,r_0)=\frac{\rho_0(r_0)D_{m,k}(r_0)}{r_0\rho_0(h)D_{m,k}(h)}\left[\frac{\partial\widehat{p}_{G,m,2}}{\partial r}(k,h)+B_{m,k}(h)\widehat{p}_{G,m,2}(k,h)\right].\tag{4.15}$$

The dispersion relation for the sonic and nearly convected modes is $K(k,r_0)=0$. Indeed, by definition, $\widehat{p}_{G,m,2}$ satisfies the wave equation and the rigid boundary condition on the outer duct wall $r=1$. If, in addition, k is the solution of $K(k,r_0)=0$,

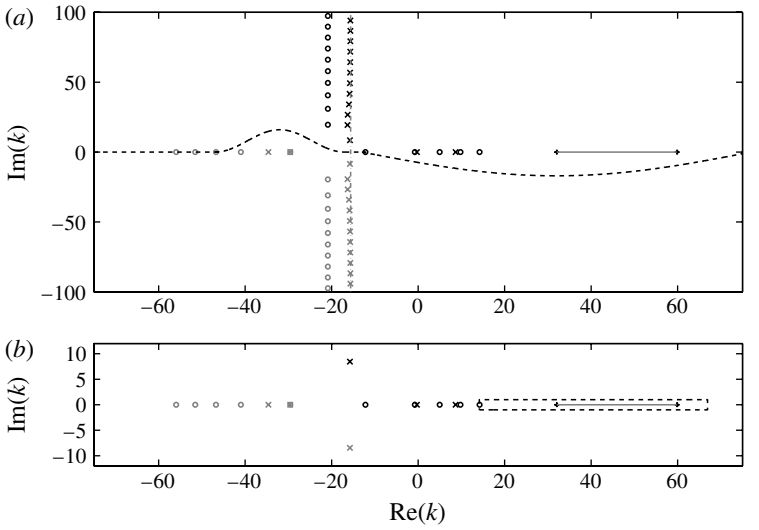

FIGURE 2. Upstream (grey) and downstream (black) sonic modes (× symbols), nearly convected modes (black + symbols) and critical layer (grey line) with swirl, and upstream (grey) and downstream (black) acoustic modes (◯ symbols) with uniform mean flow in the complex k plane for $h = 0.5$, $\omega = 30$, $m = 16$, $M_\theta(r) = 0.28r + 0.1/r$, $M_x(1) = 0.4$ and radial equilibrium. The acoustic modes in uniform mean flow (◯ symbols) are given for an average axial mean flow and speed of sound, which gives: $\omega_{unif} = 30.234$ and $M_{x,unif} = 0.5105$. (*a*) Large view, with a schematic integration contour Γ_k (black dashed line), and the asymptotic real part of the cut-off sonic modes (dashed–dotted grey line); (*b*) zoom around the real axis and actual numerical integration contour $\mathscr{C}_k$ (black dashed line). (In the studied case, the first four nearly convected modes are [32.036, 32.079] and [59.946, 59.809].).

then $\widehat{p}_{G,m,2}$ also satisfies the rigid boundary condition on the inner duct wall $r = h$, from (4.15). Namely, $k = k^{\pm}_{m,\mu}$ is an eigenvalue of the ducted swirling flow. The latter can correspond to an upstream-going sonic mode ($k = k^{+,S}_{m,\mu}$), a downstream-going sonic mode ($k = k^{-,S}_{m,\mu}$) or a downstream nearly convected mode ($k = k^{-,NC}_{m,\mu}$); see figure 2. For each family of modes, the index $\mu \in \mathbb{N}$ is the radial order. So let us introduce for convenience $\Psi^{\pm}_{m,\mu}$, the particular eigenfunction scaled so that

$$\int_0^{2\pi}\int_h^1 |\Psi^{\pm}_{m,\mu}(r)\exp(\mathrm{i}m\theta)|^2 r\,\mathrm{d}r\,\mathrm{d}\theta = \pi(1-h^2), \tag{4.16}$$

to be consistent with the dimensional norm $\pi R_T^*(1-h^2)$ used in the uniform mean flow case (e.g. by Ventres *et al.* (1982) and Posson *et al.* (2011)). Eigenfunction $\Psi^{\pm}_{m,\mu}$ satisfies

$$\widehat{p}_{G,m,1}(k^{\pm,S}_{m,\mu}, r) = \frac{\Psi^{\pm}_{m,\mu}(r)}{h\Psi^{\pm}_{m,\mu}(h)} \quad \text{and} \quad \widehat{p}_{G,m,2}(k^{\pm,S}_{m,\mu}, r) = \frac{\Psi^{\pm}_{m,\mu}(r)}{\Psi^{\pm}_{m,\mu}(1)}. \tag{4.17}$$

Let $C^{\pm}_{m,\mu} = h\Psi^{\pm}_{m,\mu}(h)\Psi^{\pm}_{m,\mu}(1)$, then

$$\widehat{p}_{G,m,1}(k^{\pm}_{m,\mu}, r_0)\widehat{p}_{G,m,2}(k^{\pm}_{m,\mu}, r) = \frac{\Psi^{\pm}_{m,\mu}(r)\Psi^{\pm}_{m,\mu}(r_0)}{C^{\pm}_{m,\mu}} = \widehat{p}_{G,m,1}(k^{\pm}_{m,\mu}, r)\widehat{p}_{G,m,2}(k^{\pm}_{m,\mu}, r_0). \tag{4.18}$$

This result will be used in §§ 4.2 and 6.

Finally, notice that the pressure-field solution of the sixth-order partial differential equation in the real time–space domain can be obtained by solving in the Fourier space (k, m, ω) a second-order ODE with respect to the radial coordinate with two boundary conditions (of rigid duct walls here), exactly as in uniform axial mean flow. As a result, this approach, using a single equation for the pressure, is expected to be computationally attractive.

4.2. *Green's function computation*

For each frequency ω and each azimuthal mode order m, the eigenvalue problem for k is first solved by a pseudo-spectral method using both the Chebyshev collocation grid and the Chebyshev staggered grid as proposed and detailed by Khorrami (1991). The four equations (2.4)–(2.7) with a zero right-hand side are Fourier-transformed in time and in the axial and tangential directions. The staggered grid is used to discretize the pressure and the axial and tangential velocity variables, whereas the radial velocity component on which the boundary conditions are defined ($u = 0$ at $r = h$ and $r = 1$) is discretized on the collocated grid. This yields the axial wavenumbers $k^{\pm}_{m,\mu}$ of the sonic and nearly convected modes. The critical layer is also investigated, and an example is plotted in figure 2. First, the critical layer (continuous grey line) lies on the real axis and is defined by $\{k_c(r) \mid \Lambda(k_c(r)) = 0 \text{ and } r \in [h, 1]\}$. Second, the modal content splits into the sonic modes ($\times$ symbols close to the acoustic modes in uniform mean flow) and the nearly convected modes (black $+$ symbols). The nearly convected modes cluster towards the ends of the critical layer. The infinitely many sonic modes split into upstream-going modes (grey) and downstream-going modes (black), among which only a finite number are cut on, as in uniform mean flow. Third, the swirl modifies the sonic-mode eigenvalues and associated cut-on frequencies, with the consistent result that fewer modes (two instead of five here) are cut on with swirl for a co-rotating mode ($m > 0$). The real part of the cut-off sonic modes also differs from that of the acoustic modes in uniform mean flow. The high-order limit of the real part of these cut-off sonic modes, as is given by Heaton & Peake (2005, equation (2.16)) in a more specific swirl, applies here (dashed–dotted vertical grey line in figure 2*a*).

To yield the pressure field in the space domain, the integration contour Γ_k, over the wavenumbers k, must be carefully defined by causality considerations using the Briggs–Bers procedure described by Heaton & Peake (2006, § 4). The continuous spectrum and the nearly convected modes must lie above Γ_k and contribute to the integral downstream of the forcing when the contour is closed in the upper half-plane. The sonic modes can originate from either $\mathrm{Im}(k) > 0$ (downstream-going propagating or evanescent modes, contributing when $x > x_0$) or $\mathrm{Im}(k) < 0$ (upstream-going propagating or evanescent modes, contributing when $x < x_0$). A resulting integration contour is illustrated in figure 2(*a*) by the dashed black curve. In practice, the integration over the wavenumber k is split into two parts. First, the contribution of each sonic mode is computed using the residue theorem. This permits a fast and accurate evaluation of the contribution of the sonic modes. It also permits us to exhibit the contribution of each mode separately to quantify their respective effects and give a result very similar to that in uniform mean flow: the contribution of a sonic duct mode (m, μ) to $\widehat{p}_{G,m}(r \mid k, \omega, \boldsymbol{x}_0, t_0)$ is

$$\begin{aligned}\widehat{p}^{\pm,S}_{G,m,\mu}(r \mid \omega, \boldsymbol{x}_0, t_0) &= \widehat{p}_{G,m}(r \mid k^{\pm,S}_{m,\mu}, \omega, \boldsymbol{x}_0, t_0)\\ &= \pm \mathrm{i} \frac{\mathrm{e}^{\mathrm{i}k^{\pm,S}_{m,\mu}(x-x_0)}\mathrm{e}^{\mathrm{i}m(\theta-\theta_0)-\mathrm{i}\omega(t-t_0)}}{(2\pi)^2 r_0 C^{\pm,S}_{m,\mu} \dfrac{\partial K}{\partial k}(k^{\pm,S}_{m,\mu}, r_0)} \Psi^{\pm,S}_{m,\mu}(r)\Psi^{\pm,S}_{m,\mu}(r_0), \qquad (4.19)\end{aligned}$$

using (4.18). The associated $G^{\pm,S}_{m,\mu}$ is obtained from (4.7). To shorten the notation, $\Lambda_{m,k^{\pm,S}_{m,\mu}}$ is written $\Lambda^{\pm,S}_{m,\mu}$, and similarly for other variables like $D_{m,k}$ and $B_{m,k}$. The derivative of K with respect to k is computed from (4.15), and reduces to

$$\frac{\partial K}{\partial k}(k^{\pm,S}_{m,\mu}, r_0) = \frac{\rho_0(r_0)D(r_0)}{r_0\rho_0(h)D(h)}\left[\frac{\partial^2 \widehat{p}_{G,m,2}}{\partial r\,\partial k}(k^{\pm,S}_{m,\mu}, h) + B^{\pm,S}_{m,\mu}(h)\frac{\partial \widehat{p}_{G,m,2}}{\partial k}(k^{\pm,S}_{m,\mu}, h) - 2\frac{mU_\theta(h)U_x(h)}{h\Lambda_{m,\mu}(h)^2}\widehat{p}_{G,m,2}(k^{\pm,S}_{m,\mu}, h)\right]. \tag{4.20}$$

Second, the contribution of the nearly convected modes and of the critical layer is obtained from a numerical evaluation of the integral around the closed contour $\mathscr{C}_k$ in the complex k plane that encloses them, as shown by the dashed black line in figure 2(*b*). Both for an eigenvalue $k = k^{\pm}_{m,\mu}$ and for k on $\mathscr{C}_k$, the two functions $\widehat{p}_{G,m,i}(k, r)$, $i = 1, 2$, are found as solutions of an initial-value problem for a system of two first-order differential equations by noting that the second-order differential operator $\mathscr{L}$ can be written as a system of two first-order equations, as described in § B.1. In addition, $\partial\widehat{p}_{G,m,2}(k^{\pm,S}_{m,\mu}, r)/\partial k$ must be evaluated to compute the contribution of the sonic modes (see (4.20)). Computing this derivative numerically, e.g. by finite differences, is time consuming and not sufficiently accurate, and instead a new system of two first-order ODEs is solved as an initial-value problem. The details are given in § B.2

If the swirl is zero and the axial flow is uniform, the sixth-order operator in (3.6) corresponds to applying the fourth-order convective derivation $\mathrm{D}^4_0/\mathrm{D}t^4$ to the wave operator in uniform mean flow, and the boundary conditions on the duct walls are exactly those in uniform mean flow: $\partial G/\partial r = 0$ at $r = h$ and $r = 1$. Furthermore, the derivatives can be swapped in $\mathscr{F}$, and $\mathrm{D}^4_0 G/\mathrm{D}t^4$ is exactly the Green's function tailored to an annular duct with uniform mean flow, as used for instance by Goldstein (1976), Ventres *et al.* (1982) and Posson *et al.* (2011).

4.3. *Implementation, assessment and sensitivity to the numerical parameters*

In this subsection we briefly describe the validation of our Green's function computations.

First, spurious eigenvalues produced by the pseudo-spectral method are discarded by application of a continuity criterion and a resolvedness criterion. The first of these removes modes that vary significantly as the number of points in the pseudo-spectral method, N, is increased, while the second removes modes for which the eigenmode is not sufficiently well resolved. Full details of this procedure are described by Brambley (2007). Furthermore, the convergence of the evaluation of the eigenvalues and the Green's function as a function of N has been checked by doubling the number of points, showing a perfect agreement for the chosen precision ($N = 200$ or $N = 100$), as observed in figure 3. Second, we have checked that both the eigenvalues and the Green's function obtained for the swirl of figure 2 vary slowly and smoothly when the swirl is varied slowly (e.g. varying Ω or Γ, other parameters being kept constant), as shown for instance in figure 3, where Ω is varied. In addition, when the swirl and axial shear have been set to zero, our computations of the eigenvalues and the Green's function are in perfect agreement with the results from the uniform mean flow case, for which the Green's function is defined analytically in terms of Bessel functions. Third, our computation of the eigenvalues has been checked by comparison with results from previous studies with non-zero swirl (e.g. Golubev & Atassi 1998;

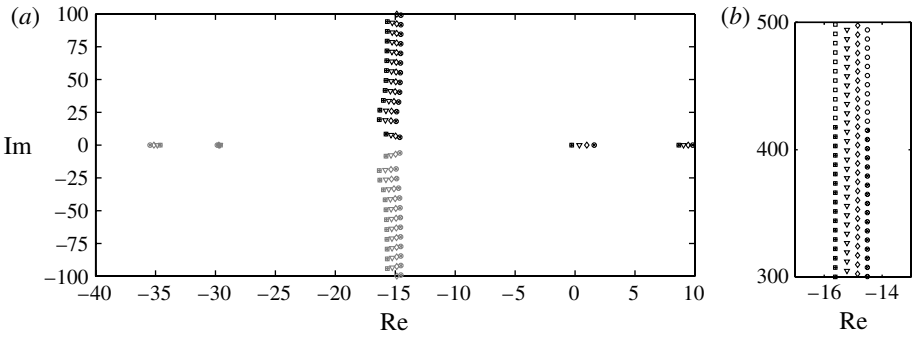

FIGURE 3. Eigenvalues obtained for different $\Omega = \{0.28; 0.26; 0.24; 0.22\}$ with $\Gamma = 0.1$ and $M_{xd}(R_T) = 0.4$ with a radial equilibrium as in figure 2. For $N = 200$: $\Omega = 0.28$ (squares), $\Omega = 0.26$ (triangles), $\Omega = 0.24$ (diamonds), $\Omega = 0.22$ (circles). For $N = 100$: $\Omega = 0.28$ (pluses), $\Omega = 0.22$ (crosses).

Heaton & Peake 2005, 2006), and in particular the nearly convected modes are well predicted in each of the three kinds of accumulation found by Heaton & Peake (2006). The present Green's function is closely related to Heaton & Peake's (2006) Green's function, and, once the differences have been accounted for, we obtain complete agreement with these previous results.

5. Pressure-field solution of the governing equation

Having found the Green's function, we can now solve (3.5) for the pressure p. First, define a generalized Green's function $\widetilde{G}$ equal to G in the region defined by $f \geqslant 0$, and taking any value in the region defined by $f < 0$. Then, p is given by

$$p(\boldsymbol{x}, t) = \iiiint_V \widetilde{G}(\boldsymbol{x}, t \,|\, \boldsymbol{x}_0, t_0)(\widetilde{\mathbb{S}}(\boldsymbol{x}_0, t_0) + \mathbb{S}_{FWH}(\boldsymbol{x}_0, t_0)) r_0 \,\mathrm{d}\theta_0 \,\mathrm{d}r_0 \,\mathrm{d}x_0 \,\mathrm{d}t_0, \tag{5.1}$$

where V is the whole space. This expression is true whatever the value of $\widetilde{G}$ is in $f < 0$, because no sources of noise (volume or surface) are included in $f < 0$. We can now write p as a sum of contributions from volume and surface terms, respectively,

$$p(\boldsymbol{x}, t) = T_V(\boldsymbol{x}, t) + T_S(\boldsymbol{x}, t), \tag{5.2}$$

with

$$T_V(\boldsymbol{x}, t) = \iiiint_V \widetilde{G}(\boldsymbol{x}, t \,|\, \boldsymbol{x}_0, t_0)(\mathscr{A}_0(\widetilde{\mathbb{S}}_1) + \mathscr{D}_0^2(\widetilde{\mathbb{S}}_2))(\boldsymbol{x}_0, t_0) \,\mathrm{d}V_0 \,\mathrm{d}t_0 \tag{5.3}$$

and

$$T_S(\boldsymbol{x}, t) = \iiiint_V \widetilde{G}(\boldsymbol{x}, t \,|\, \boldsymbol{x}_0, t_0)(\mathscr{A}_0(\mathbb{S}_{FWH,1}) + \mathscr{D}_0^2(\mathbb{S}_{FWH,2}))(\boldsymbol{x}_0, t_0) \,\mathrm{d}V_0 \,\mathrm{d}t_0, \tag{5.4}$$

where the subscript 0 on the operators $\mathscr{A}$ and $\mathscr{D}$ means that the derivatives in the operator $\mathscr{A}$ defined by (3.8) and $\mathscr{D}$ defined by (A 5) are performed with respect to the source time t_0 and space coordinates $\boldsymbol{x}_0$, instead of with respect to the observer variables t and $\boldsymbol{x}$. The next step is to perform sufficiently many integrations by parts in (5.4) to remove all derivatives from the terms $\mathbb{S}_{FWH,i}$ so as to be able to use the Dirac delta distribution to complete integrals over the surfaces defined by $f = 0$, and

similarly in (5.3) so as to uncover the Heaviside function and obtain an integral over the fluid volume $\mathscr{V}$. The final expression for T_S is

$$\begin{aligned} T_S(\boldsymbol{x},t) = &+\iiint_{\Sigma_B(t_0)} \boldsymbol{S}_{FWH}\cdot\nabla(\mathscr{D}_0^2(G)) - S_{FWH,\rho}\frac{\mathrm{D}_0}{\mathrm{D}t_0}(\mathscr{D}_0^2(G))\,\mathrm{d}\Sigma_0(t_0)\,\mathrm{d}t_0 \\ &+\iiint_{\Sigma_B(t_0)} 2S_{FWH,\theta}\frac{U_\theta}{r_0}\mathscr{R}_{0,1}(G)\,\mathrm{d}\Sigma_0(t_0)\,\mathrm{d}t_0 \\ &+\iiint_{\Sigma_B(t_0)} S_{FWH,r}\mathscr{R}_{0,2}(G)\,\mathrm{d}\Sigma_0(t_0)\,\mathrm{d}t_0, \end{aligned} \tag{5.5}$$

where the operators $\mathscr{R}_{0,1}$ and $\mathscr{R}_{0,2}$ are defined in appendix C. The surface integrals in (5.5) reduce to integrals over the blade surfaces. Indeed, it can be shown that the surface integral along the duct walls is zero if we use the tailored Green's function derived in the previous section and neglect the acoustic pressure generated by the viscous stresses on the inner and outer duct walls. This result generalizes the result in uniform base flow; the first integral in (5.5) is analogous to the result obtained by Goldstein (1976) for a uniform base flow. If there is no swirl nor any radial shear of the axial mean flow, then the last two integrals in (5.5) are zero and $\mathscr{D}_0^2(G)$ reduces to the Green's function tailored to an annular duct in a uniform base flow. The second integral in (5.5) is caused by the swirl and is associated with the force on the blade in the azimuthal direction. The third integral in (5.5) is caused by either swirl or shear (see (C 2)) and is associated with the force on the blade in the radial direction. As a result, if the viscous force on the blade is neglected and the blades are aligned radially this last integral is zero.

The final expression for the volume term T_V is

$$\begin{aligned} T_V = &+\iiiint_{\mathscr{V}(t_0)} Z\left\{\frac{\mathrm{D}_0^2}{\mathrm{D}t_0^2} - c_0^2\nabla^2\right\}[\mathscr{D}_0^2(G)] + T_{ij}\frac{\partial^2}{\partial y_i\,\partial y_j}[\mathscr{D}_0^2(G)]\,\mathrm{d}V_0\,\mathrm{d}t_0 \\ &-\iiiint_{\mathscr{V}(t_0)} \nabla(\mathscr{D}_0^2(G))\cdot\left[\rho\mathcal{H} + \frac{U_\theta^2}{r_0}Z\boldsymbol{e_r}\right] \\ &+\rho u\left[\frac{\mathrm{d}U_x}{\mathrm{d}r_0}\frac{\partial}{\partial x_0} + \frac{\mathrm{d}}{\mathrm{d}r_0}\left[\frac{U_\theta}{r_0}\right]\frac{\partial}{\partial\theta_0}\right](\mathscr{D}_0^2(G))\,\mathrm{d}V_0\,\mathrm{d}t_0 \\ &-\iiiint_{\mathscr{V}(t_0)} 2\frac{U_\theta}{r_0}\left[\overline{\overline{\boldsymbol{\tau}}}\cdot(\nabla[\mathscr{R}_{0,1}(\widetilde{G})])\right. \\ &\left.+\mathscr{R}_{0,1}(\widetilde{G})\left(\rho_{to}(\boldsymbol{u}\cdot\nabla)\boldsymbol{u} + \rho\frac{\mathrm{D}_0\boldsymbol{u}}{\mathrm{D}t_0} + \rho\mathcal{H}\right)\right]\cdot\boldsymbol{e_\theta}\,\mathrm{d}V_0\,\mathrm{d}t_0 \\ &-\iiiint_{\mathscr{V}(t_0)} \left[\overline{\overline{\boldsymbol{\tau}}}\cdot(\nabla[\mathscr{R}_{0,2}(\widetilde{G})]) + \mathscr{R}_{0,2}(\widetilde{G})\right. \\ &\left.\times\left(\rho_{to}(\boldsymbol{u}\cdot\nabla)\boldsymbol{u} + \rho\frac{\mathrm{D}_0\boldsymbol{u}}{\mathrm{D}t_0} + \rho\mathcal{H} + \frac{U_\theta^2}{r_0}Z\boldsymbol{e_r}\right)\right]\cdot\boldsymbol{e_r}\,\mathrm{d}V_0\,\mathrm{d}t_0. \end{aligned} \tag{5.6}$$

The first integral in (5.6) is analogous to the usual quadrupole term in a medium at rest or in a uniform mean flow (see (3.12)). We recall that, since we write down an equation for the pressure rather than the fluctuating density, we find also the first term in the first integral in (5.6) involving the non-isentropic variable Z. Every integrand in the other three integrals in (5.6) is proportional to at least one of U_θ, $\mathrm{d}U_\theta/\mathrm{d}r$ or $\mathrm{d}U_x/\mathrm{d}r$, and so they are zero in a uniform non-swirling base flow.

Finally, note that the integration by parts has allowed us to move all the derivatives from the source terms onto the Green's function. This is an important practical point, because calculating higher-order derivatives of the sources, which have themselves been obtained with limited precision from computational fluid dynamics (CFD) or experiment, is a clear source of error. As a result, in our formulation one may expect not to need any extra precision in the evaluation of the noise sources than what is required in uniform mean flow. (For instance, in the following section, only the blade pressure distribution will have to be evaluated, just as is required in uniform mean flow case when considering subsonic turbomachinery noise.) On the other hand, it might appear that there is some increased difficulty in computing the derivatives of the Green's function compared to the uniform flow. However, since we Fourier-transform in time and in axial and azimuthal directions, only the first and second derivatives in r are required numerically, but in fact, given the way that our Green's function computation has been set up, these radial derivatives are actually rather easy to obtain accurately – see appendix B.

6. Pressure-field solution in the particular case of subsonic rotor noise

The above developments are now applied to the problem of noise generation by the rotor of an aeroengine fan stage. The flow upstream of the rotor is almost uniform (in practice, some shear is observed because of the duct wall boundary layers and distortion in the ingested flow, but this will be neglected here). The rotor has rotational speed Ω_R, and downstream of the rotor the mean flow has swirl of azimuthal component $U_\theta(r)$ and radially varying axial component $U_x(r)$. We choose to investigate here very general axial mean flow profiles (defined as a sum of a polynomial and a rational polynomial in r). However, an axial mean flow profile defined by radial equilibrium and assuming that the stagnation enthalpy is constant and the fluid is homentropic (e.g. Golubev & Atassi 2000*a*,*b*) could also be studied with the present acoustic analogy.

6.1. *Assumptions and general result*

We will neglect the contribution of the volume integral T_V in (5.2), as is usually done in this context for subsonic blade speed (e.g. Goldstein 1976, § 4.3). However, in a uniform mean flow configuration, Morfey (1971), for instance, suggests that the quadrupole terms may be important even at moderate subsonic Mach numbers, and Goldstein, Dittmar & Gelder (1974) proposed a model to include their contribution for fan inflow distortion tone noise. As a result, further investigation will be required to evaluate the effect of the term T_V as a function of the axial and azimuthal Mach numbers and to determine to what extent the swirl modifies the weight of the quadrupole terms. The blade surfaces are supposed to be impermeable and non-vibrating: $(\boldsymbol{U} + \boldsymbol{u} - \boldsymbol{V}^{\Sigma_B}) \cdot \boldsymbol{n} = 0$. The term associated with $S_{FWH,\rho}$ is related to the thickness noise or volume displacement effect, and, in the case of subsonic blade relative Mach number, Goldstein (1976, para. 4.3.2) showed that this noise is cut off in the duct with zero swirl. Since only the co-rotating modes of azimuthal order $m = sB$, with s a positive integer, are radiated, this result still holds when swirl is added. As a result, only the loading noise will be investigated here. The effect of the viscous stress tensor is neglected, $\overline{\overline{\boldsymbol{\tau}}} \cong 0$, so $\overline{\overline{\boldsymbol{L}}} \cdot \boldsymbol{n} = p\boldsymbol{n}$. Finally, the blades are assumed to be purely radial (zero lean and sweep angles), i.e. of radial blade normal component $n_r = 0$, merely to simplify the calculations. The orientation of the normals and the main blade

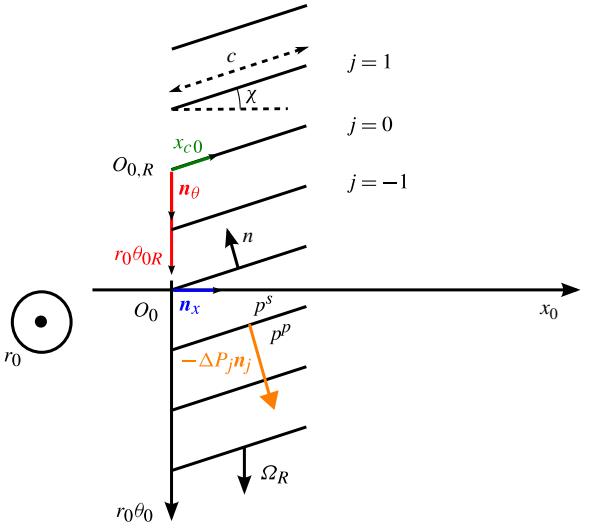

FIGURE 4. (Colour online) Sketch of the rotor in an unwrapped view at radius r, including the coordinate systems.

parameters are defined by

$$(n_r, n_\theta, n_x) = (0, -\cos\chi, -\sin\chi) = (0, -q_2, q_1), \tag{6.1}$$

as in the sketch in figure 4, where χ is the blade stagger angle and (q_1, q_2) are simply introduced to be in line with previous cascade models (Hanson 2001*b*; Posson 2008; Posson, Moreau & Roger 2010*a*; Posson *et al.* 2011). As a result of these assumptions, the pressure field is found from (5.5) by an integration over the blade surface of the product of the blade pressure distribution and a derivative operator $\mathscr{T}_0$ acting on G, i.e.

$$p(\boldsymbol{x}, t) = \iiint_{\bigcup_j \Sigma_{B,j}(t_0)} p(\boldsymbol{x}_0, t_0)\, \mathscr{T}_0(G(\boldsymbol{x}, t \,|\, \boldsymbol{x}_0, t_0))\, \mathrm{d}\Sigma_0(t_0)\, \mathrm{d}t_0, \tag{6.2}$$

with

$$\mathscr{T}_0(G) = \left[n_{x,j} \mathscr{D}_0^2 \frac{\partial G}{\partial x_0} + n_{\theta,j} \left(\frac{\mathscr{D}_0^2}{r_0} \frac{\partial G}{\partial \theta_0} + 2 \frac{U_\theta}{r_0} \mathscr{R}_{0,1}(G) \right) \right]. \tag{6.3}$$

It is now possible to use the same strategy as was done previously in uniform mean flow (e.g. Goldstein 1976; Ventres *et al.* 1982; Posson *et al.* 2011) to compute the noise generated, by simply providing the blade pressure distribution as input from an analytical model or a CFD simulation. Equation (6.2) reduces to that derived by Goldstein (1976) in a uniform mean flow case applied to an annular cross-section (e.g. Ventres *et al.* 1982; Posson *et al.* 2011) instead of a circular section (Goldstein 1976). Indeed, in this particular case, $\mathscr{T}_0(G) \equiv \boldsymbol{n} \cdot \boldsymbol{\nabla}(\mathrm{D}_0^4 G / \mathrm{D}t_0^4)$ and $\mathrm{D}_0^4 G / \mathrm{D}t_0^4 = G_{unif}$ is exactly the Green's function tailored to a rigid annular duct with uniform axial mean flow.

In the following, the pressure distribution on the two blade surfaces (suction side p^s, pressure side p^p) will be given by an analytical model in terms of a pressure jump distribution across the blade, neglecting the effects of thickness and camber,

$$[p^s(\boldsymbol{x}_0, t_0) - p^p(\boldsymbol{x}_0, t_0)]\, \mathrm{d}S_j\, \boldsymbol{n}_j = -\Delta P_j(\boldsymbol{x}_0, t_0)\, \mathrm{d}S_j\, \boldsymbol{n}_j, \tag{6.4}$$

as sketched in figure 4, where j is the index of the current blade. As is usually done in uniform mean flow (e.g. Goldstein 1976; Ventres *et al.* 1982), the surface integral in (6.2) is evaluated in the reference frame $\mathscr{R}_R$ of the rotor. By definition, $\theta_0 = \theta_{0R} + \Omega_R t_0$, where θ_{0R} is the angular position of a point $\boldsymbol{x}_0$ (denoted $\boldsymbol{x}_{0,\boldsymbol{R}} = (r_0, \theta_{0R}, x_0)$) in $\mathscr{R}_R$. The Fourier decomposition (4.2) of the Green's function is introduced, and the time and space integrals are switched. Then $\Delta\widehat{P}_j(\boldsymbol{x}_{0,\boldsymbol{R}}, \omega)$, the Fourier transform in time of the pressure jump across the blade j, and $\mathscr{T}_{m,k,r_0}$, the time and axial Fourier transform and azimuthal Fourier series of the operator $\mathscr{T}_0$ defined by (6.3), are introduced to write the pressure field as

$$p(\boldsymbol{x}, t) = 2\pi\mathrm{i} \int_\omega \sum_{m\in\mathbb{Z}} \int_k \iint_{\bigcup_j S_j} \Delta\widehat{P}_j(\boldsymbol{x}_{0,\boldsymbol{R}}, \omega_m)\, \mathscr{T}_{m,k,r_0}(\widehat{\widehat{G}}_m(r \,|\, k, \omega, r_0)) \times \mathrm{e}^{\mathrm{i}k(x-x_0)+\mathrm{i}m(\theta-\theta_{0R,j})-\mathrm{i}\omega t}\, \mathrm{d}S_{0,j}\, \mathrm{d}k\, \mathrm{d}\omega, \tag{6.5}$$

with $\omega_m = \omega - m\Omega_R$. The noise radiated in mode m at frequency ω is caused by noise sources at frequency ω_m. For each frequency ω and azimuthal order m, the pressure-field components can be split as the sum of the contribution $P^{\pm,S}_{m,\mu}(\boldsymbol{x}, t \,|\, \omega)$ of the sonic modes (m, μ) and the contribution $P^{-,NCCL}_m(\boldsymbol{x}, t \,|\, \omega)$ of the sum of the nearly convected modes plus the critical layer obtained by numerical integration over $k \in \mathscr{C}_k$ of $P^{-,NCCL}_m(\boldsymbol{x}, t \,|\, \omega, k)$. The exponent $\pm$ stands for the field radiated upstream $(+)$ and downstream $(-)$ of the blade row. Note that the nearly convected modes and the critical layer only contribute downstream of the sources, as explained in § 4.2.

After some algebra, the contribution of a sonic mode (m, μ) reads

$$P^{\pm,S}_{m,\mu}(\boldsymbol{x}, t \,|\, \omega) = \mathscr{P}^{\pm,S}_{m,\mu}(\omega)\Psi^{\pm}_{m,\mu}(r)\mathrm{e}^{\mathrm{i}k^{\pm,S}_{m,\mu}x+\mathrm{i}m\theta-\mathrm{i}\omega t}, \tag{6.6}$$

with

$$\mathscr{P}^{\pm,S}_{m,\mu}(\omega) = \sum_{j=0}^{B-1} \mathrm{e}^{\mathrm{i}(2\pi mj/B)} \int_h^1 \int_0^{c(r_0)} \Delta\widehat{P}_j(\boldsymbol{x}_{0,\boldsymbol{R}}, \omega_m) S^{\pm}_{m,\mu}(\omega, r_0)\, \mathrm{e}^{-\mathrm{i}k^{\pm,S}_{m,\mu,c}x_{c0}}\, \mathrm{d}x_{c0}\, \mathrm{d}r_0 \tag{6.7}$$

and

$$S^{\pm}_{m,\mu}(\omega, r_0) = \pm \frac{1}{2\pi C^{\pm}_{m,\mu} r_0 \dfrac{\partial K}{\partial k}(k^{\pm,S}_{m,\mu}, r_0)} \left\{ \left(q_2 \frac{m}{r_0} - q_1 k^{\pm,S}_{m,\mu} \right) \frac{D^{\pm,S}_{m,\mu}(r_0)}{\Lambda^{\pm,S}_{m,\mu}(r_0)^2} \Psi^{\pm}_{m,\mu}(r_0) + \frac{2q_2 U_\theta}{r_0 \Lambda^{\pm,S}_{m,\mu}(r_0)} \left[B^{\pm,S}_{m,\mu}(r_0)\Psi^{\pm}_{m,\mu}(r_0) + \frac{\mathrm{d}\Psi^{\pm}_{m,\mu}(r_0)}{\mathrm{d}r_0} \right] \right\}. \tag{6.8}$$

Here $k^{\pm,S}_{m,\mu,c} = k^{\pm,S}_{m,\mu} \cos\chi - (m/r_0)\sin\chi$ is the chordwise wavenumber.

Similarly, the overall contribution of the nearly convected modes and the critical layer is

$$P^{-,NCCL}_m(\boldsymbol{x}, t \,|\, \omega) = \int_{\mathscr{C}_k} P^{-,NCCL}_m(r \,|\, \omega, k)\, \mathrm{e}^{\mathrm{i}kx+\mathrm{i}m\theta-\mathrm{i}\omega t}\, \mathrm{d}k, \tag{6.9}$$

with

$$P^{-,NCCL}_m(r \,|\, \omega, k) = \sum_{j=0}^{B-1} \mathrm{e}^{+\mathrm{i}(2\pi mj/B)} \int_h^1 \int_0^{c(r_0)} \Delta\widehat{P}_j(\boldsymbol{x}_{0,\boldsymbol{R}}, \omega_m) S^{-}_{m}(\omega, k, r_0)\, \mathrm{e}^{-\mathrm{i}k_c x_{c0}}\, \mathrm{d}x_{c0}\, \mathrm{d}r_0 \tag{6.10}$$

and

$$S_m^-(\omega, k, r_0) = \mathrm{i}\left\{\left(q_2\frac{m}{r_0} - q_1 k\right)\frac{D_{m,k}(r_0)}{\Lambda_{m,k}(r_0)^2}\widehat{M}_m + \frac{2U_\theta q_2}{r_0\Lambda_{m,k}(r_0)}\left[\frac{\partial\widehat{M}_m}{\partial r_0} + \left(\frac{2mU_\theta}{r_0^2\Lambda_{m,k}(r_0)} + \frac{1}{D_{m,k}(r_0)}\frac{\mathrm{d}D_{m,k}(r_0)}{\mathrm{d}r_0}\right)\widehat{M}_m\right]\right\}. \tag{6.11}$$

In (6.10), $k_c = k\cos\chi - (m/r_0)\sin\chi$, and if $r > r_0$ then

$$\widehat{M}_m(r\,|\,k, \omega, r_0) = +\frac{1}{(2\pi)^2 r_0 K(k, r_0)}\widehat{p}_{G,m,1}(k, r_0)\widehat{p}_{G,m,2}(k, r), \tag{6.12}$$

and the term in square brackets in (6.11) is equal to

$$\frac{1}{(2\pi)^2 r_0 K(k, r_0)}\frac{\partial\widehat{p}_{G,m,1}}{\partial r_0}(k, r_0)\widehat{p}_{G,m,2}(k, r) + B_{m,k}\widehat{M}_m, \tag{6.13}$$

whereas if $r < r_0$ then

$$\widehat{M}_m(r\,|\,k, \omega, r_0) = +\frac{1}{(2\pi)^2 r_0 K(k, r_0)}\widehat{p}_{G,m,2}(k, r_0)\widehat{p}_{G,m,1}(k, r), \tag{6.14}$$

and the term in square brackets in (6.11) is equal to

$$\frac{1}{(2\pi)^2 r_0 K(k, r_0)}\frac{\partial\widehat{p}_{G,m,2}}{\partial r_0}(k, r_0)\widehat{p}_{G,m,1}(k, r) + B_{m,k}\widehat{M}_m. \tag{6.15}$$

6.2. *Specific case of the rotor tonal noise*

We believe that the effects of swirling flow must be included in a number of key noise sources, including rotor-alone broadband noise and rotor–stator interaction noise. The application of our new result (5.2), (5.5) and (5.6) in these contexts will be described in later papers (see Posson & Peake (2012) for preliminary results in the rotor-alone case). However, both these cases require significant additional technical elaboration. So in order to exhibit the effect of swirl, we consider in this paper the simpler case of the noise produced by the interaction of an upstream steady non-uniform flow with the fan. This may be caused by installation effects such as the presence of the wing, or ingested turbulence (Goldstein 1976), and is believed to be a significant noise source in certain configurations (see e.g. Koch 2012).

6.2.1. *Formulation*

To illustrate the effect of the swirl, an inflow obstacle upstream of the rotor is supposed to produce a stationary mean Gaussian wake of half-width θ_0 and depth αU_x^∞ inside the uniform axial mean flow U_x^∞ coming from upstream infinity. The total incident steady non-uniform flow is

$$\boldsymbol{u}_{inc}(\boldsymbol{x}) = U_x^\infty(1 - \alpha\,\mathrm{e}^{-\ln 2(\theta/\theta_0)^2})\boldsymbol{e}_x = \sum_{q\in\mathbb{Z}} u_q\,\mathrm{e}^{\mathrm{i}q\theta}\boldsymbol{e}_x, \tag{6.16}$$

with Fourier coefficients $u_q = \delta_{q0} - \{(\alpha\theta_0)/(2\sqrt{(\pi\ln 2)})\}\exp[-(q\theta_0/2)^2/\ln 2]$. The analytical blade response model used is only sensitive to the fluctuation w of the incoming velocity in the direction normal to the blade, i.e. of the Fourier coefficients $w_q = -u_q\sin\chi_R$ (since $\boldsymbol{u}_{inc}$ is purely axial). In practice, all the following results

are obtained for $\alpha = 40\,\%$, a half-width $\theta_0 = \pi/20$, taking at most $q \in [-30, 30]$. A uniform upstream mean flow is defined by taking the average axial mean flow component of the swirling mean flow (to be specified in due course) downstream of the rotor and dividing by the square root of the average square speed of sound, i.e. defined in non-dimensional variables by $c_{0,unif} = \mathrm{mean}(c_0(r)^2)^{1/2}$ and $U_{x,unif} = \mathrm{mean}(U_x(r))/c_{0,unif}$. Similarly the density in uniform mean flow is defined from an average of that with swirl. This uniform mean flow is used to define $U_x^\infty = U_{x,unif}$ and $c_0^\infty = c_{0,unif}$.

Since each blade rotates in the direction of the increasing θ_0 at speed Ω_R, the perturbation rotates in the direction of decreasing θ_{0R} at Ω_R in the reference frame $\mathscr{R}_R$ fixed to the rotor, and the blade loading fluctuates periodically at frequency Ω_R. A Fourier series in time is performed and the space–time periodicity properties are used to give the pressure jump across blade j,

$$\begin{aligned}\Delta P_j(\boldsymbol{x}_{0,\boldsymbol{R}}, t_0) &= \Delta P(x_0, r_0, \theta_{0R,j}, t_0) = \Delta P\left(x_0, r_0, \theta_{0R,0} - \frac{2\pi}{B}j, t_0\right)\\ &= \Delta P\left(x_0, r_0, \theta_{0R,0}, t_0 - \frac{2\pi}{B\Omega_R}j\right)\\ &= \Delta P_0\left(\boldsymbol{x}_{0,\boldsymbol{R}}, t_0 - \frac{2\pi}{B\Omega_R}j\right)\end{aligned} \tag{6.17}$$

and

$$\Delta P_j(\boldsymbol{x}_{0,\boldsymbol{R}}, t_0) = \sum_{q\in\mathbb{Z}} \Delta\widehat{P}_{q,0}(\boldsymbol{x}_{0,\boldsymbol{R}})\, \mathrm{e}^{\mathrm{i}(2\pi q/B)j}\, \mathrm{e}^{-\mathrm{i}q\Omega_R t_0}, \tag{6.18}$$

where $\Delta\widehat{P}_{q,0}(\boldsymbol{x}_{0,\boldsymbol{R}})$ is the time Fourier series harmonic of order q of the pressure jump on blade 0 corresponding to the loading at frequency $q\,\Omega_R$ that is produced by the harmonic q of the flow distortion w_q. For identical equi-spaced blades, m and q satisfy the well-known Tyler & Sofrin (1962) condition $m + q = sB$, $s \in \mathbb{Z}$, and finally

$$p(\boldsymbol{x}, t) = \sum_{s\in\mathbb{Z}} \widehat{p}_{sB}(\boldsymbol{x})\, \mathrm{e}^{-\mathrm{i}sB\Omega_R t}, \tag{6.19}$$

with

$$\begin{aligned}\widehat{p}_{sB}(\boldsymbol{x}) = 2\mathrm{i}\pi B \sum_{q\in\mathbb{Z}} \iint_{S_0} \Delta\widehat{P}_{q,0}(\boldsymbol{x}_{0,\boldsymbol{R}}) \int_k \mathscr{T}_{m,k,r_0}(\widehat{\widehat{G}}_m(r \mid k, sB\Omega_R, r_0))\\ \times\, \mathrm{e}^{\mathrm{i}k(x-x_0)}\, \mathrm{d}k\, \mathrm{e}^{-\mathrm{i}m\theta_{0R,0}}\, \mathrm{d}S_{0,0}\, \mathrm{e}^{\mathrm{i}m\theta}.\end{aligned} \tag{6.20}$$

We have therefore obtained the well-known result that the non-uniform mean flow–rotor interaction noise is produced at a multiple of the blade passing frequency (BPF, $sB\Omega_R$), and is the sum of the contributions of dipole noise sources (pressure jump distribution) at the harmonics of the rotation ($q\Omega_R$), and these noise sources contribute to the duct mode of azimuthal order $m = sB - q$ (if it is cut on at $\omega = sB\Omega_R$). Then, for each frequency ω and azimuthal order m, the pressure-field components can be split as the sum of the contribution of the sonic modes and the contribution of the sum of the nearly convected modes plus the critical layer as detailed in § 6.1. The expression is given by setting $\omega = sB\Omega_R$ ($\omega_m = q\Omega_R$) and $m = sB - q$ in the final results (equations (6.6) and (6.9)) of § 6.1.

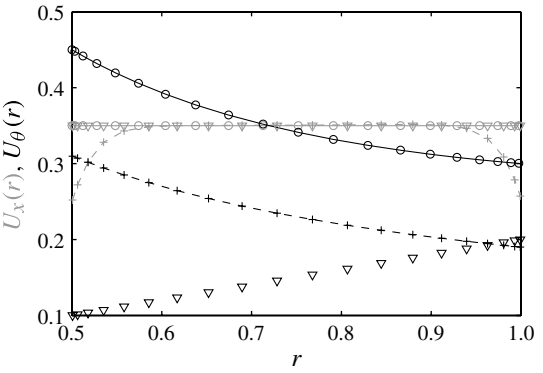

FIGURE 5. Radial profile of the axial $U_x(r)$ (grey) and tangential $U_\theta(r)$ (black) non-dimensional mean flow components in configuration with swirl (RS) defined in table 1: case (I) triangles, (II) solid lines with circles and (III) dashed lines with crosses.

In practice, the unsteady blade loading response to a fluctuation of the velocity field in its reference frame is computed using the unsteady blade response function of Posson, Roger & Moreau (2010*b*) based on Glegg's (1999) cascade response model. Since the purpose is to illustrate the effect of the swirling mean flow, only two-dimensional gusts are considered for simplicity. The spanwise variation of the mean flow fluctuations are only accounted for parametrically in the amplitude $w_q(r)$. The required inputs at each strip are the gust amplitude $w_q(r)$, the frequency $\omega = q\Omega_R$, the inter-blade phase angle $\sigma = 2\pi q/B$, the local chord $c_d(r)$ and stagger angle $\chi(r)$, and the local mean flow Mach number along the blade $M = U_{xd}^\infty/(c_0^\infty \cos(\chi(r)))$.

6.2.2. *Test case*

Our test case is inspired by the rotor geometry and the mean flow downstream of the rotor at approach condition of the 22-inch Source Diagnostic Test (SDT) fan rig of the NASA Glenn Research Center (Hughes *et al.* 2002; Podboy *et al.* 2002*a*). The rotor has $B = 22$ blades, the hub-to-tip ratio $h = 0.5$, the non-dimensional chord is constant $c_d = 0.3$, and the stagger angle varies linearly from hub to tip between 20 and 55°. Three different swirling mean flows downstream of the rotor are investigated. They are defined in table 1, and their profiles are plotted in figure 5: case (I) is solid-body swirl; case (II) is a rather general swirl involving both a solid body and a free vortex; and case (III) corresponds to a realistic swirl for the studied rotor at approach condition inspired by the SDT results, involving both swirl and a sheared flow caused by the boundary layers. We look at the first harmonic of the BPF ($s = 2$), which corresponds to a non-dimensional frequency $\omega = sB\Omega_R = 30$, and consider all the cut-on modes m that are excited, i.e. $m = sB - q$ for $q \in [-30, 30]$. The extremal values of the cut-on and excited m in each case are given in the last column of table 1. However, in practice, the response for $|q| > 27$ is negligible.

A calculation using the actual swirl and the acoustic analogy derived in this paper will be referred to as (RS). In order to evaluate the effect of swirling mean flow, the above-defined uniform mean flow $U_{x,unif}$ is also investigated. Its values are given in the second column of table 1. The calculations performed with a uniform mean flow and the associated acoustic analogy (Goldstein 1976; Ventres *et al.* 1982) will be referred to as (UF). In a third calculation, the swirl effect is approximated by a simple Doppler shift in the frequencies while using the above-defined uniform mean flow, as

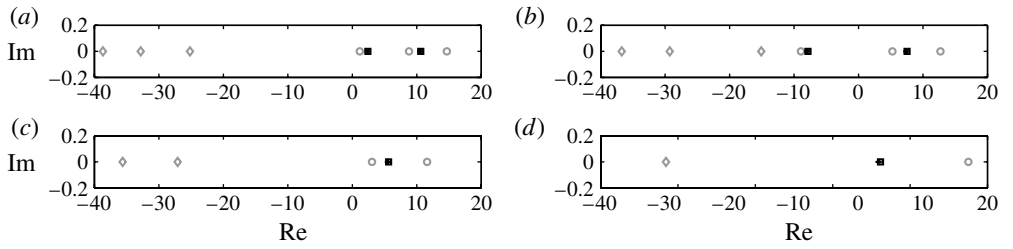

FIGURE 6. Eigenvalues in case (I) for the azimuthal mode orders (*a*) $m = 18$, (*b*) $m = 20$, (*c*) $m = 21$ and (*d*) $m = 24$. Downstream eigenvalues obtained with (RS) (black squares), (DC) (black crosses) and (UF) (grey circles); and upstream eigenvalues with (UF) (grey diamonds).

Case	$U_{x,unif}$	$U_x(r)$	$U_\theta(r)$	$m = sB - q$
(I)	0.351	0.35	$0.2\,r$	(UF) $\in [14, 29]$ (DC) $\in [14, 24]$ (RS) $\in [14, 24]$
(II)	0.352	0.35	$0.1\,r + 0.2/r$	(UF) $\in [14, 29]$ (DC) $\in [14, 22]$ (RS) $\in [14, 22]$
(III)	0.343	$0.35 - 0.1\left(\dfrac{2r-1-h}{2(1-h)}\right)^{10}$	$\dfrac{0.12}{r} + 0.07$	(UF) $\in [14, 29]$ (DC) $\in [14, 24]$ (RS) $\in [14, 24]$

TABLE 1. Definition of the parameters of the tonal noise test cases. UF = uniform mean flow, DC = Doppler effect correction, RS = real swirl.

proposed by Topol (1999), i.e. the duct mode eigenvalues and eigenvectors, and, as a result, the duct mode cut-on frequency, the duct mode axial wavenumber and radial shapes are computed using a uniform mean flow but replacing the actual frequency $\omega/c_{0,unif}$ by $(\omega - mU_\theta/r)/c_{0,unif}$. In practice, since $U_\theta(r)/r$ is not constant (except for a solid-body swirl), we chose in the present paper $(\omega - mU_\theta(1))/c_{0,unif}$. This approach will be referred to as Doppler effect correction (DC), and is often thought of as a way of dealing with the swirling mean flow effect in a very simple way (Topol 1999; Hanson 2001*a*; Posson & Moreau 2011). Its actual validity will be investigated here by comparison with our full solution.

6.2.3. *Results*

The axial wavenumbers of the downstream-going cut-on sonic modes are plotted in each of the three flow configurations (I)–(III) in figures 6–8, respectively. The number of cut-on modes (m, μ) for m fixed tends to decrease with swirl; for instance, in case (II) there are four, three and two cut-on modes in uniform mean flow at $m = 17$, $m \in [18, 20]$ and $m \in [21, 22]$, respectively, whereas there are only two at $m = 17$ and one at $m \in [18, 22]$ with swirl. The maximal azimuthal mode order m of a cut-on mode is also decreased, as reported in the last column of table 1, where the mode $m = 29$ is cut on in uniform mean flow whereas modes $m > 25$ are all cut off with

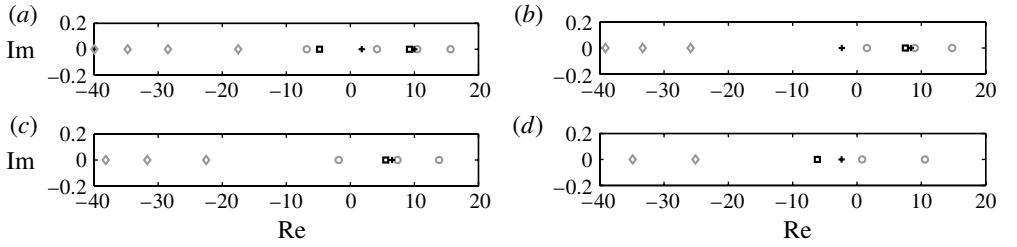

FIGURE 7. Eigenvalues in case (II) for the azimuthal mode orders (*a*) $m = 17$, (*b*) $m = 18$, (*c*) $m = 19$ and (*d*) $m = 22$. Downstream eigenvalues obtained with (RS) (black squares), (DC) (black crosses) and (UF) (grey circles); and upstream eigenvalues with (UF) (grey diamonds).

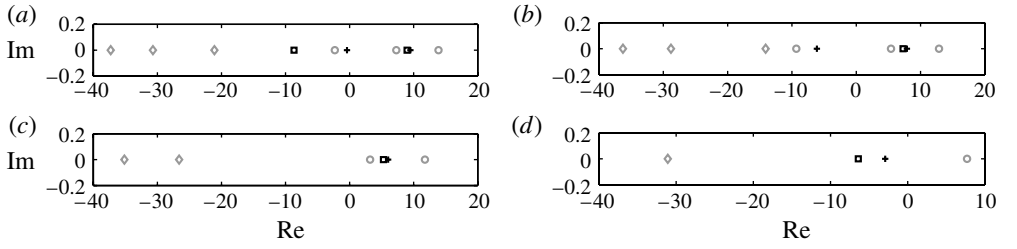

FIGURE 8. Eigenvalues in case (III) for the azimuthal mode orders (*a*) $m = 19$, (*b*) $m = 20$, (*c*) $m = 21$ and (*d*) $m = 24$. Downstream eigenvalues obtained with (RS) (black squares), (DC) (black crosses) and (UF) (grey circles); and upstream eigenvalues with (UF) (grey diamonds).

swirl. This is the well-known result that swirling mean flow increases the cut-on frequency of co-rotating modes ($m > 0$).

If a solid-body swirl is considered as in case (I), the Doppler effect correction predicts accurately the wavenumbers, as in figure 6, where the square and plus symbols almost lie on top of each other. This is no longer the case for more general flows, as in cases (II) and (III) in figures 7 and 8. The wavenumbers are no longer the same, and the cut-on frequency is also changed, which can lead to a different number of cut-on modes. For $m = 18$ in case (II) in figure 7(*b*) and for $m = 20$ in case (III) in figure 8(*b*), the (DC) predicts two cut-on modes $\mu = 0$ and $\mu = 1$ whereas only the mode $\mu = 0$ is still cut on with the actual swirl.

Before investigating the pressure field generated by the interaction of the blades with the non-uniform mean flow, the Green's functions are compared in the case (II), corresponding to a solid-body plus a free-vortex swirl. Since in uniform mean flow the Green's function is $\mathrm{D}_0^4 G/\mathrm{D}t_0^4 = G_{unif}$, we do not compare directly the two Green's function but we compare a downstream sonic mode (m, μ) component $\widehat{p}^{-,S}_{G,m,\mu}$, part of the Green's function $G^{-,S}_{m,\mu}$ (obtained from (4.19)), with the modal component (m, μ) of the uniform mean flow Green's function

$$G^{-}_{m,\mu,unif} = \frac{\mathrm{i}}{4\pi} \frac{E_{m\mu}(r) E_{m\mu}(r_0)}{\Gamma_{m\mu} \kappa_{m\mu}} \mathrm{e}^{\mathrm{i}k^{\pm}_{m\mu}(x-x_0)} \mathrm{e}^{\mathrm{i}m(\theta-\theta_0)}. \tag{6.21}$$

In addition, the result obtained with the Doppler effect correction and the overall contribution of the nearly convected modes and critical layer for this m are also plotted

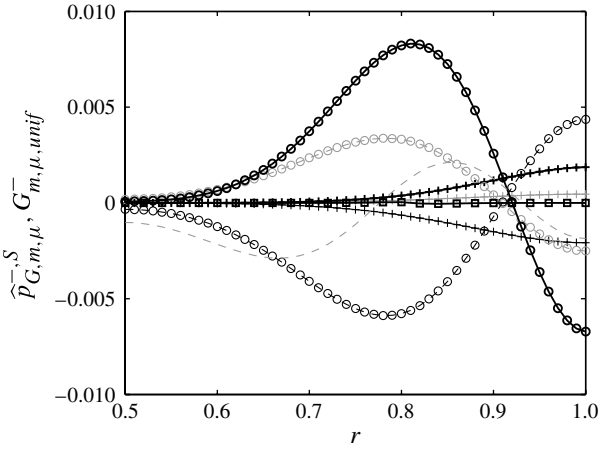

FIGURE 9. Radial profiles of modal components (m, μ) of the Green's function for $m = 17$ at $(x, \theta) = (0.4, 0)$ for a point source at $(r_0, \theta_0, x_0) = (0.82, 0, 0.0)$ computed with (UF) (grey lines), with (RS) (black thick lines) and with (DC) (black thin lines) for $\mu = 0$ (plus symbols), $\mu = 1$ (circles) and $\mu = 2$ (dashed lines, only UF). The contribution of NCCL is plotted in thick lines with squares.

in figure 9. The plots in figure 9 are radial profiles obtained at one chordwise position $x = 0.4$ and azimuthal position $\theta = 0$ for a point source at $(r_0, \theta_0, x_0) = (0.82, 0, 0.0)$. The swirling mean flow changes not only the number of cut-on modes, as emphasized previously, but also the amplitude of the contribution of each mode. The nearly convected modes and the critical layer have a negligible contribution to the Green's function, and they also have no perceptible effect on the radiated pressure for the cases studied. They will not be plotted in the following. This result is very helpful, because the computation of their contribution is extremely time-consuming compared to the computation of the sonic modes. There are two reasons for this. First, the contour $\mathscr{C}_k$ in (6.9) must be sufficiently far from the nearly convected modes and critical layer to avoid rapid oscillation, and therefore the numerical evaluation over this relatively long contour needs a substantial number of points. Second, the integration of the unsteady blade loading times the phase term $\exp(\mathrm{i}k_c(x - x_0))$ along the blade chord requires computation of a double integral in x_0 and k, and, while an analytical expression for the integration with respect to x_0 exists for the sonic modes, the integral must be performed fully numerically for k on $\mathscr{C}_k$. This is hardly tractable when many axial positions x are computed for colour maps over all possible m. Additional study of the effect of the nearly convected modes and critical layer (NCCL) has been performed by Posson & Peake (2012) for a single azimuthal mode order m with a point dipole source $x_0 = 0$ at each radial location. In that study no perceptible effect of NCCL was observed when the swirl is a solid body and/or free vortex with a uniform axial flow or a flow in radial equilibrium. However, when considering the test case proposed in Heaton & Peake (2006, § 3.3), both an algebraically unstable continuous spectrum and unstable nearly convected modes are found, and the pressure field exhibits a downstream growth of the amplitude and an increase in its spanwise spatial extent. Even so, the amplitude at four tip radii downstream remains small. In the context of a fan, the axial extent of the engine may not be sufficient for the amplitude and the spatial extent of this unstable perturbation to have a significant effect, and it still seems

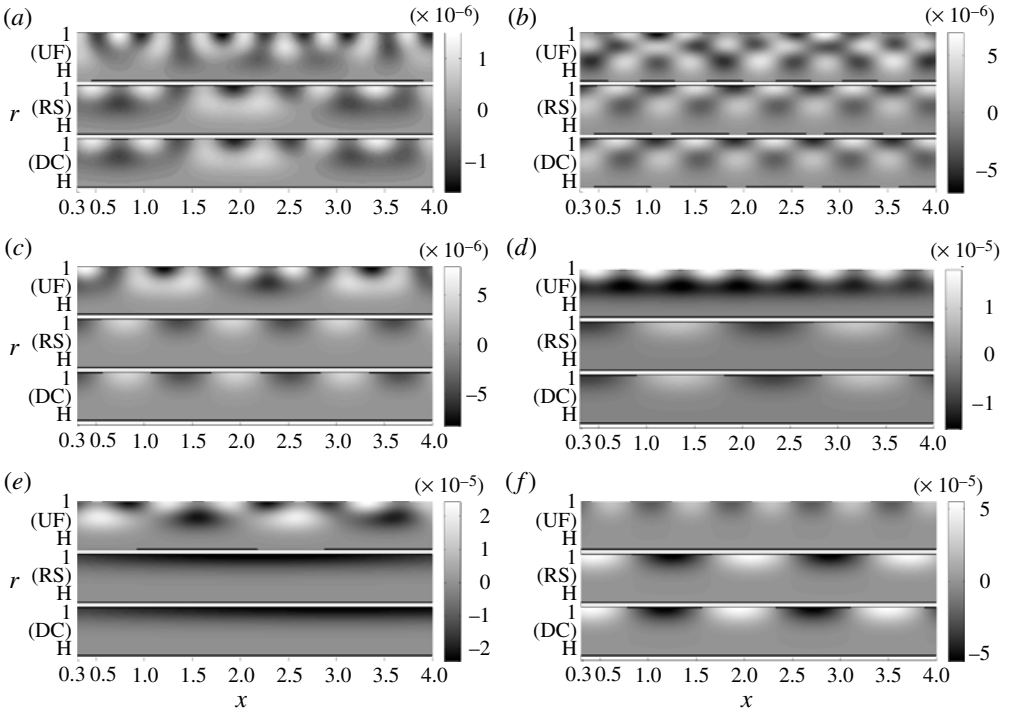

FIGURE 10. Radiated pressure field in mode (*a*) $m = 18$, (*b*) $m = 20$, (*c*) $m = 21$, (*d*) $m = 22$, (*e*) $m = 23$ and (*f*) $m = 24$, in case (I), obtained with (UF) (top), with the sonic mode from (RS) (middle) and with (DC) (bottom) in each panel.

reasonable to neglect the NCCL contribution. However, the nearly convected modes and the critical layer are expected to contribute to the acoustic power if diffracting surfaces are present (splitter, other blade row, etc.). In a future work, it would then be necessary to investigate the efficiency of the diffraction of these perturbations by the stator to make a final conclusion about their effect.

Colour maps of the pressure field radiated downstream of the rotor are plotted in figures 10, 11 and 13 for the cases (I)–(III), respectively. Each panel corresponds to a specific azimuthal order m and contains three colour maps corresponding to the pressure field in the duct downstream of the rotor produced using a uniform mean flow (UF, top), the sonic mode contribution from a real swirl using our present theory (RS, middle), and the result from a Doppler effect correction (DC, bottom). In all the cases studied, the pressure pattern obtained in swirling mean flow (RS) is very different from that with uniform mean flow (UF) for the same azimuthal order. In addition, the (UF) contains a significant part of the pressure field in modes $m \in [25, 29]$, as shown in figure 12 for $m = 27$. As a result, the swirling mean flow tends to decrease the overall pressure amplitude, mostly because only co-rotating modes are excited for this fan inflow distortion tone noise. This will no longer be the case for rotor–stator interaction noise, because contra-rotating modes, which tend to be cut on by swirl, will also be excited. Note that results close to a cut-on frequency must be considered with care because specific treatments should be applied to the analytical model which provides the unsteady blade loading (e.g. Posson & Roger 2011). It is then expected that the effect of the modes m close to their cut-on frequency is overestimated in the

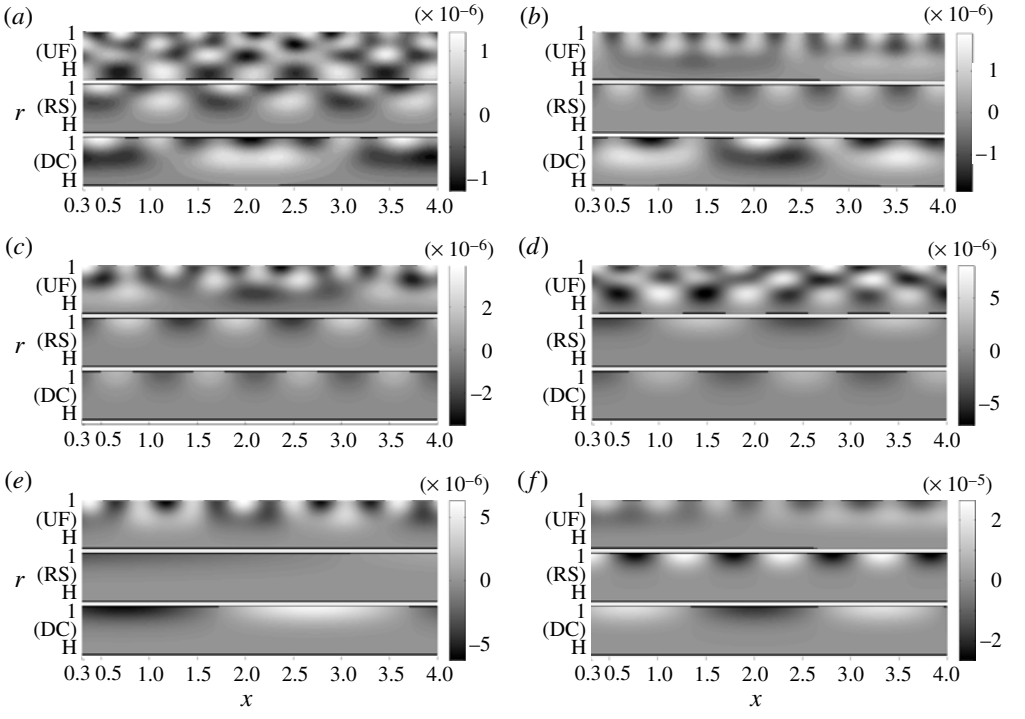

FIGURE 11. Radiated pressure field in mode (*a*) $m = 17$, (*b*) $m = 18$, (*c*) $m = 19$, (*d*) $m = 20$, (*e*) $m = 21$ and (*f*) $m = 22$, in case (II), obtained with (UF) (top), with the sonic mode from (RS) (middle) and with (DC) (bottom) in each panel.

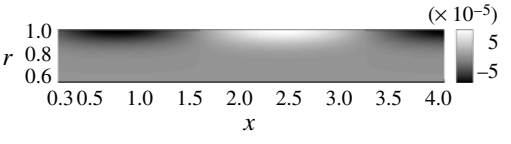

FIGURE 12. Radiated pressure field in mode $m = 27$ in uniform mean flow from case (II).

present study because the analytical model has been used in its two-dimensional form. This is probably the case for $m = 29$ in uniform mean flow in all cases and for $m = 18$ with (RS) in figure 13(*a*). In other words, the sources may not be fully accurate, but we emphasize that the Green's function itself is properly computed.

The solid-body swirl of case (I) of table 1 is investigated in figure 10. The result obtained with a simple Doppler effect correction gives very good results, with very small discrepancies observed only for the higher mode order $m = 24$. A complementary study performed with a radial line of dipoles by Posson & Peake (2012) tends to the same conclusion, even if the discrepancies observed in that study were slightly more pronounced. They also observed that at low azimuthal order (e.g. $m = 5$ not excited here) the swirl has no noticeable effect either on the wavenumbers or on the radiated pressure field with solid-body swirl. In this highly idealized case, the Doppler effect correction can be used to predict the effect of swirl.

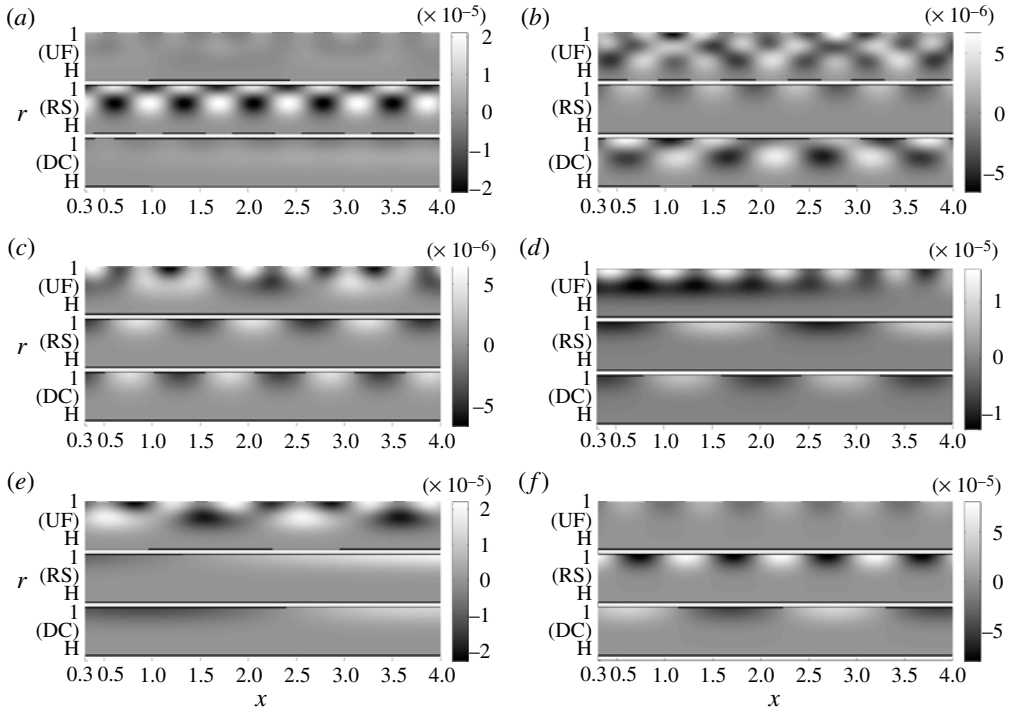

FIGURE 13. Radiated pressure field in mode (*a*) $m = 19$, (*b*) $m = 20$, (*c*) $m = 21$, (*d*) $m = 22$, (*e*) $m = 23$ and (*f*) $m = 24$, in case (III), obtained with (UF) (top), with the sonic mode from (RS) (middle) and with (DC) (bottom) in each panel.

A more realistic swirl, corresponding to the case (II) of table 1 involving both solid-body swirl and free-vortex swirl, is studied in figure 11. In this case, the Doppler effect correction (DC) is no longer able to capture the pressure-field pattern. This is certainly the case, and is to be expected, for azimuthal mode orders for which the number of cut-on modes differs between (RS) and (DC) such as in figure 11(*b*) for $m = 18$ (see figure 7*b*), and when the wavenumbers are very different, such as $m = 21$ and 22 in figure 11(*e*,*f*) (see figure 7*d*). However, even when the modes are far from their cut-on frequency and the wavenumbers are quite close, such as $m = 19$ and 20 in figure 11(*c*,*d*) (see figure 7*c*), significant discrepancies between (RS) and (DC) are observed.

Finally, a realistic swirl, inspired by the actual flow measured in the SDT case (Hughes *et al.* 2002; Podboy *et al.* 2002*a*; Envia *et al.* 2008) at approach condition, is investigated in figure 13. As in the previous case, the effect of the swirling mean flow is strong when comparing the results with (RS) and without (UF) swirl, and the Doppler effect correction is unable to capture the acoustic behaviour. To quantify the overall effect of the swirl and the limitation of the Doppler effect correction, the overall pressure field obtained by summing up the contribution of all the cut-on sonic modes is plotted in figure 14(*a*). The maximum pressure levels found in the domains shown are 6.43×10^{-5} and 9.68×10^{-5} for the Doppler effect correction and the real swirl, respectively, with $m_{max} = 24$, and 7.39×10^{-4} for the uniform mean flow case with $m_{max} = 29$ (if only the contribution of the modes $m \leqslant 24$ were considered, the maximum pressure would have been 4.35×10^{-5}). This result shows the strong

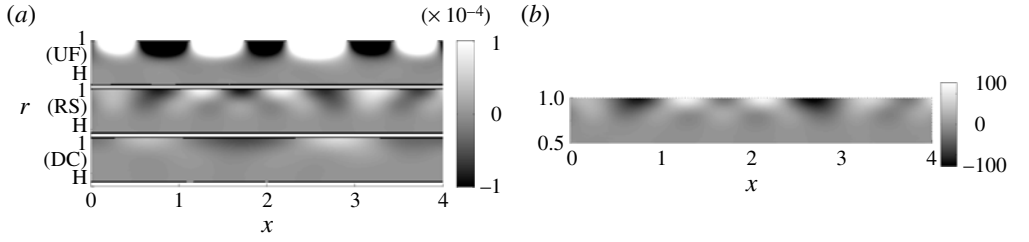

FIGURE 14. (*a*) Overall radiated pressure field in case (III), obtained with (UF) (top), with the sonic mode from (RS) (middle) and with (DC) (bottom). (*b*) Error in per cent between (DC) and (RS): plotted variable is $100[(\mathrm{RS}) - (\mathrm{DC})]/\max|(\mathrm{RS})|$.

difference between the uniform flow case and the swirl. It also gives some clues on the limitation of the Doppler correction compared to the actual swirl. The associated percentage error between the Doppler effect correction and the real swirl is plotted in figure 14(*b*), showing a relative error of up to 137 %. These results underline the necessity of using an acoustic analogy that takes full account of the swirl, as developed in this paper, rather than using the simplified Doppler effect correction, for realistic flows. The possible strong effect of the swirl and the limitation of the Doppler effect correction was also observed and emphasized by Posson & Peake (2012) for the prediction of rotor trailing-edge noise for a realist flow field and blade geometry.

7. Conclusion

In this paper we have developed an acoustic analogy to predict sound generation in a swirling and sheared flow in an annular duct, including the presence of (possibly moving) solid surfaces to account for rotor and stator blades. In so doing we have extended a number of classical earlier results, including Ffowcs Williams & Hawkings' (1969) equation in a medium at rest with moving surfaces, Goldstein's (1976) acoustic analogy for a circular duct with uniform axial mean flow, and Lilley's (1974) equation for a sheared but non-swirling jet. Our approach has involved considering perturbations about an axisymmetric swirling and sheared base state, and then rearranging the Navier–Stokes equations into the form of a single sixth-order differential operator in time and space acting on the fluctuating pressure field on the left-hand side, with the remaining terms representing a series of volume and surface source terms on the right-hand side (equation (3.5)). The solution of this equation for the acoustic pressure can then be cast into integral form, and we use the tailored Green's function for swirling flow in a rigid annular duct (the numerical calculation of which is described) so that the source contributions are limited to the volume of the fluid and the blade surfaces. These source contributions include not only the familiar Lighthill quadrupole volume sources and the momentum and volume displacement surface sources, but also a series of new terms that arise only in swirling flow. For instance, the blade surface contribution (equation (5.5)), which is often thought to be dominant in turbomachinery flow, contains three terms: the first term is analogous to the result obtained by Goldstein (1976) for a uniform base flow, and reduces to it with no swirl or shear; the second term, which involves the blade forces in the azimuthal direction, arises only in swirl; and the third term, which involves the radial component of the blade force, arises in either swirl or radial shear.

Our new theory can be used for a range of turbomachinery noise sources which are affected by swirling flow, including rotor-alone trailing-edge broadband noise and rotor–stator (broadband and tonal) interaction noise. In this paper we have considered as a first step the noise produced by the interaction of a steady non-uniform flow entering the fan to illustrate the possible effect of the swirl on an academic problem, involving gusts. A series of different mean flows were considered, and in all these cases the swirl is shown to modify the pressure distribution downstream of the fan. When the swirl is simply solid-body rotation, introducing an elementary Doppler effect correction when computing the duct modes in uniform mean flow is sufficient to predict accurately the noise radiated with swirl. However, for more realistic flows the effect of the swirl can only be included using the full swirling-flow acoustic analogy, as developed in this paper. The present acoustic analogy has also been applied to the problem of rotor trailing-edge noise by Posson & Peake (2012), who showed preliminary results on the effects of the swirl on rotor trailing-edge noise while using simplified rotor trailing-edge noise sources (in particular, not including cascade effects). This problem will be considered in a further publication with a more advanced trailing-edge noise model and comparisons with experimental data.

In addition to the further work mentioned above, there is the possibility for extending our work in a number of other directions. Here we have used an analytical model for the blade response, but of course computational approaches could equally well be used to provide the surface source terms. The volume source terms, neglected in the first instance here, could also be modelled (computationally or semi-analytically), and it would be interesting to investigate whether their contribution remains smaller than the surface terms when swirling and/or sheared flow is included. Consideration of non-isentropic base flows could also be important, especially given the increasing interest in turbine noise. The assumption of constant mean flow along the axial direction may not be valid in general, especially for low-frequency noise, as was shown by Karabasov *et al.* (2010) and recently by Goldstein, Sescu & Afsar (2012) for jet noise. It may be possible to extend the present study to a slowly axially varying mean flow and duct section using a multiple scales approach as proposed for instance by Rienstra (1999), although implementation of this method for the purpose of the derivation of an acoustic analogy may be rather complicated. Finally, if the assumption of axially slowly varying mean flow is no longer valid, a more general acoustic analogy such as that of Goldstein *et al.* (2012) or even a full numerical computation should be considered.

Appendix A. Derivation of the sixth-order partial differential equation for the fluctuating pressure field

To derive a single equation for the pressure, we proceed as follows. First, the axial and tangential components of the fluctuating velocity w and v are eliminated from the system (3.2). The convective derivative $\mathrm{D}_0/\mathrm{D}t$ is applied first to the mass conservation equation and second to the momentum equation in the radial direction of the system (3.2) to yield

$$\frac{1}{c_0^2}\frac{\mathrm{D}_0^2 p}{\mathrm{D}t^2}+\rho_0\frac{\mathrm{D}_0 u}{\mathrm{D}t}\left(\frac{1}{\rho_0}\frac{\mathrm{d}\rho_0}{\mathrm{d}r}+\frac{1}{r}\right)+\rho_0\frac{\mathrm{D}_0}{\mathrm{D}t}\left(\frac{\partial u}{\partial r}\right)+\rho_0\frac{\partial}{r\partial\theta}\left(\frac{\mathrm{D}_0 v}{\mathrm{D}t}\right)+\rho_0\frac{\partial}{\partial x}\left(\frac{\mathrm{D}_0 w}{\mathrm{D}t}\right)$$
$$=\frac{\mathrm{D}_0}{\mathrm{D}t}(\widetilde{S}_\rho+S_{FWH,\rho}\delta(f)) \qquad \text{(A 1)}$$

and

$$\rho_0 \frac{\mathrm{D}_0^2 u}{\mathrm{D}t^2} - 2\frac{U_\theta}{r}\left(\rho_0 \frac{\mathrm{D}_0 v}{\mathrm{D}t}\right) = \frac{U_\theta^2}{r c_0^2}\frac{\mathrm{D}_0 p}{\mathrm{D}t} - \frac{\mathrm{D}_0}{\mathrm{D}t}\left(\frac{\partial p}{\partial r}\right) + \frac{\mathrm{D}_0}{\mathrm{D}t}(\widetilde{S}_r + S_{FWH,r}\delta(f)). \quad (A\,2)$$

Then, inserting the tangential derivative $\partial/(r\,\partial\theta)$ of the tangential momentum equation and the axial derivative $\partial/\partial x$ of the axial momentum equation into (A 1) gives

$$\begin{aligned}\frac{\mathrm{D}_0}{\mathrm{D}t}\left[\frac{\partial u}{\partial r} + \left(\frac{1}{\rho_0}\frac{\mathrm{d}\rho_0}{\mathrm{d}r} + \frac{1}{r}\right)u\right] - \frac{\mathrm{d}(rU_\theta)}{r\,\mathrm{d}r}\frac{\partial u}{r\,\partial\theta} - \frac{\mathrm{d}U_x}{\mathrm{d}r}\frac{\partial u}{\partial x} \\ = \frac{1}{\rho_0}\left[\frac{\partial^2 p}{r^2\,\partial\theta^2} + \frac{\partial^2 p}{\partial x^2} - \frac{1}{c_0^2}\frac{\mathrm{D}_0^2 p}{\mathrm{D}t^2}\right] + \frac{1}{\rho_0}[\widetilde{\mathbb{S}}_2 + \mathbb{S}_{FWH,2}],\end{aligned} \quad (A\,3)$$

and inserting the tangential momentum equation into (A 2) gives

$$\mathscr{M}(p) = \rho_0\,\mathscr{D}(u) + \widetilde{\mathbb{S}}_1 + \mathbb{S}_{FWH,1}, \quad (A\,4)$$

with

$$\mathscr{M}(p) = \frac{\mathrm{D}_0}{\mathrm{D}t}\left(\frac{\partial p}{\partial r}\right) + 2\frac{U_\theta}{r^2}\frac{\partial p}{\partial\theta} - \frac{U_\theta^2}{r c_0^2}\frac{\mathrm{D}_0 p}{\mathrm{D}t} \quad \text{and} \quad \mathscr{D}(u) = -\frac{\mathrm{D}_0^2 u}{\mathrm{D}t^2} - 2\frac{U_\theta}{r^2}\frac{\mathrm{d}(rU_\theta)}{\mathrm{d}r}u. \quad (A\,5)$$

In (A 3) and (A 4) the source terms are given by (3.9) and (3.10). We have therefore eliminated w and v. The next step is to differentiate (A 3) and (A 4) to remove any dependence on u. Let us first note that

$$\begin{aligned}\frac{\partial}{\partial r}(\mathscr{D}(u)) = \mathscr{D}\left(\frac{\partial u}{\partial r}\right) - 2\frac{\mathrm{D}_0}{\mathrm{D}t}\left[\frac{\mathrm{d}U_x}{\mathrm{d}r}\frac{\partial}{\partial x} + \frac{\mathrm{d}}{\mathrm{d}r}\left(\frac{U_\theta}{r}\right)\frac{\partial}{\partial\theta}\right]u \\ - \frac{\mathrm{d}}{\mathrm{d}r}\left[\frac{2U_\theta}{r^2}\frac{\mathrm{d}(rU_\theta)}{\mathrm{d}r}\right]u,\end{aligned} \quad (A\,6)$$

so that applying the operator $\mathscr{D}$ to (A 3) leads to

$$\begin{aligned}\frac{\mathrm{D}_0}{\mathrm{D}t}\left(\frac{\partial}{\partial r}[\mathscr{D}(u)]\right) = -\frac{1}{\rho_0}\left[\left(\frac{1}{\rho_0}\frac{\mathrm{d}\rho_0}{\mathrm{d}r} + \frac{1}{r}\right)\frac{\mathrm{D}_0}{\mathrm{D}t} - \frac{\mathrm{d}(rU_\theta)}{r\,\mathrm{d}r}\frac{\partial}{r\,\partial\theta} - \frac{\mathrm{d}U_x}{\mathrm{d}r}\frac{\partial}{\partial x}\right]\rho_0\mathscr{D}(u) \\ + \frac{1}{\rho_0}\left[\frac{\partial^2}{r^2\,\partial\theta^2} + \frac{\partial^2}{\partial x^2} - \frac{1}{c_0^2}\frac{\mathrm{D}_0^2}{\mathrm{D}t^2}\right]\mathscr{D}(p) + \frac{1}{\rho_0}\mathscr{D}(\widetilde{\mathbb{S}}_2 + \mathbb{S}_{FWH,2}) \\ - 2\frac{\mathrm{D}_0^2}{\mathrm{D}t^2}\left[\frac{\mathrm{d}U_x}{\mathrm{d}r}\frac{\partial}{\partial x} + \frac{\mathrm{d}}{\mathrm{d}r}\left(\frac{U_\theta}{r}\right)\frac{\partial}{\partial\theta}\right]u - \frac{\mathrm{d}}{\mathrm{d}r}\left[\frac{2U_\theta}{r^2}\frac{\mathrm{d}(rU_\theta)}{\mathrm{d}r}\right]\frac{\mathrm{D}_0 u}{\mathrm{D}t}.\end{aligned} \quad (A\,7)$$

Taking the radial derivative of (A 4) and applying the convective derivative operator to the resulting equation gives

$$\begin{aligned}\frac{\mathrm{D}_0}{\mathrm{D}t}\left(\frac{\partial}{\partial r}(\mathscr{M}(p))\right) = \frac{1}{\rho_0}\frac{\mathrm{d}\rho_0}{\mathrm{d}r}\frac{\mathrm{D}_0}{\mathrm{D}t}(\mathscr{M}(p) - \widetilde{\mathbb{S}}_1 - \mathbb{S}_{FWH,1}) + \rho_0\frac{\mathrm{D}_0}{\mathrm{D}t}\left(\frac{\partial}{\partial r}(\mathscr{D}(u))\right) \\ + \frac{\mathrm{D}_0}{\mathrm{D}t}\left(\frac{\partial}{\partial r}[\widetilde{\mathbb{S}}_1 + \mathbb{S}_{FWH,1}]\right).\end{aligned} \quad (A\,8)$$

Our next step is to eliminate $\mathrm{D}_0[\partial[\mathscr{D}(u)]/\partial r]/\mathrm{D}t$ in the second term on the right-hand side of (A 8) by using (A 6), to give

$$\begin{aligned}\frac{\mathrm{D}_0}{\mathrm{D}t}\left(\frac{\partial}{\partial r}(\mathscr{M}(p))\right) = &-\left[\frac{1}{r}\frac{\mathrm{D}_0}{\mathrm{D}t} - \frac{\mathrm{d}(rU_\theta)}{r\,\mathrm{d}r}\frac{\partial}{r\,\partial\theta} - \frac{\mathrm{d}U_x}{\mathrm{d}r}\frac{\partial}{\partial x}\right][\mathscr{M}(p) - \widetilde{\mathbb{S}}_1 - \mathbb{S}_{FWH,1}]\\ &+\left[\frac{\partial^2}{r^2\,\partial\theta^2} + \frac{\partial^2}{\partial x^2} - \frac{1}{c_0^2}\frac{\mathrm{D}_0^2}{\mathrm{D}t^2}\right]\mathscr{D}(p)\\ &+\mathscr{D}(\widetilde{\mathbb{S}}_2 + \mathbb{S}_{FWH,2}) + \frac{\mathrm{D}_0}{\mathrm{D}t}\left(\frac{\partial}{\partial r}[\widetilde{\mathbb{S}}_1 + \mathbb{S}_{FWH,1}]\right)\\ &-\left\{2\frac{\mathrm{D}_0^2}{\mathrm{D}t^2}\left[\frac{\mathrm{d}U_x}{\mathrm{d}r}\frac{\partial}{\partial x} + \frac{\mathrm{d}}{\mathrm{d}r}\left(\frac{U_\theta}{r}\right)\frac{\partial}{\partial\theta}\right]\right.\\ &\left.+\frac{\mathrm{d}}{\mathrm{d}r}\left[\frac{2U_\theta}{r^2}\frac{\mathrm{d}(rU_\theta)}{\mathrm{d}r}\right]\frac{\mathrm{D}_0}{\mathrm{D}t}\right\}\rho_0\,u. \end{aligned} \tag{A 9}$$

Finally, applying the operator $\mathscr{D}$ to (A 9) and using the relation (A 4) to eliminate u gives us the result reported in (3.5), (3.6), (3.7) and (3.8).

Appendix B. Green's function computation

B.1. *Functions $\widehat{p}_{G,m,i}(k, r_0)$ and their radial derivative*

The computation of the Green's function in § 4.2 requires us to find $\widehat{p}_{G,m,i}(k, r_0)$, $i = 1, 2$, which are the solutions of the homogeneous equation $\mathscr{L}(\widehat{p}) = 0$ that satisfy, respectively, the boundary conditions (4.12) and (4.13). For effective numerical calculation, the homogeneous problem $\mathscr{L}(\widetilde{p}) = 0$, where the operator $\mathscr{L}$ is given by (4.4), can be integrated in vector form by writing

$$\mathbb{Z} = \begin{pmatrix} z_1 \\ z_2 \end{pmatrix} = \begin{pmatrix} r\widehat{p}_{G,m,i} \\ \dfrac{r}{D_{m,k}}\left(B_{m,k}\widehat{p}_{G,m,i} + \dfrac{\mathrm{d}\widehat{p}_{G,m,i}}{\mathrm{d}r}\right) \end{pmatrix}, \tag{B 1}$$

which leads us to solve

$$\begin{pmatrix} \dfrac{\mathrm{d}z_1}{\mathrm{d}r} \\ \dfrac{\mathrm{d}z_2}{\mathrm{d}r} \end{pmatrix} = \begin{pmatrix} \dfrac{1}{r} - B_{m,k} & D_{m,k} \\ -\dfrac{1}{\Lambda_{m,k}^2}\left(\dfrac{\Lambda_{m,k}^2}{c_0^2} - \dfrac{m^2}{r^2} - k^2\right) & \dfrac{2mU_\theta}{\Lambda_{m,k}r^2} \end{pmatrix}\begin{pmatrix} z_1 \\ z_2 \end{pmatrix} = \mathbb{L}\mathbb{Z} \tag{B 2}$$

using an initial-value solver, marching from $r = h$ to $r = 1$ with the initial-value condition $\mathbb{Z}(h) = (1; 0)$ for $\widehat{p}_{G,m,1}(k, r_0)$; and marching from $r = 1$ to $r = h$ with the initial-value condition $\mathbb{Z}(1) = (1; 0)$ for $\widehat{p}_{G,m,2}(k, r_0)$.

B.2. *The k derivative of the function $\widehat{p}_{G,m,2}(k, r_0)$ and their radial derivative*

By definition, the function $(k, r) \mapsto \widehat{p}_{G,m,2}(k, r)$ is a solution of $D_{m,k}(r)\mathscr{L}_m(\widehat{p}_{G,m,2}) = 0$, which can also be written as

$$\frac{\partial^2\widehat{p}_{G,m,2}}{\partial r^2}(k, r) + A(k, m, r, \omega)\frac{\partial\widehat{p}_{G,m,2}}{\partial r}(k, r) + B(k, m, r, \omega)\widehat{p}_{G,m,2}(k, r) = 0, \tag{B 3}$$

with

$$A(k, m, r, \omega) = \frac{1}{r}\left(1 - \frac{U_\theta^2}{c_0^2}\right) - \frac{1}{D_{m,k}}\frac{\mathrm{d}D_{m,k}}{\mathrm{d}r}, \tag{B 4a}$$

$$B(k,m,r,\omega) = -\frac{2mU_\theta}{r^2\Lambda_{m,k}}\left[\frac{1}{r}+\frac{1}{D_{m,k}}\frac{\mathrm{d}D_{m,k}}{\mathrm{d}r}-\frac{1}{U_\theta}\frac{\mathrm{d}U_\theta}{\mathrm{d}r}-\frac{U_\theta^2}{rc_0^2}+\frac{k}{\Lambda_{m,k}}\frac{\mathrm{d}U_x}{\mathrm{d}r}\right] + \frac{U_\theta^2}{rc_0^2D_{m,k}}\frac{\mathrm{d}D_{m,k}}{\mathrm{d}r}+\frac{D_{m,k}}{c_0^2}-\frac{m^2}{r^2}-\frac{1}{r}\frac{\mathrm{d}}{\mathrm{d}r}\left(\frac{U_\theta^2}{c_0^2}\right)-\frac{D_{m,k}k^2}{\Lambda_{m,k}^2}, \quad \text{(B 4}b\text{)}$$

and satisfies the boundary condition (4.13). Equations (B 3) and (4.13) are theoretically valid for every pair (k,r) with k away from the critical layer and $r\in[h,1]$. In addition, they can be differentiated with respect to k in this domain. Let $\widehat{q}_{G,m,2}$ be

$$\widehat{q}^{\pm,S}_{G,m,2} = \frac{\partial\widehat{p}_{G,m,2}}{\partial k}(k^{\pm,S}_{m,\mu},r). \quad \text{(B 5)}$$

Then, the derivative with respect to k of (B 3) and (4.13) reads

$$\begin{cases} \dfrac{\mathrm{d}^2\widehat{q}^{\pm,S}_{G,m,2}}{\mathrm{d}r^2}(r)+A(k^{\pm,S}_{m,\mu},m,r,\omega)\dfrac{\mathrm{d}\widehat{q}^{\pm,S}_{G,m,2}}{\mathrm{d}r}(r)+B(k^{\pm,S}_{m,\mu},m,r,\omega)\widehat{q}^{\pm,S}_{G,m,2}(r) \\ \quad = -\dfrac{\partial A}{\partial k}(k^{\pm,S}_{m,\mu},m,r,\omega)\dfrac{\partial\widetilde{p}_{G,m,2}}{\partial r}(k^{\pm,S}_{m,\mu},r)-\dfrac{\partial B}{\partial k}(k^{\pm,S}_{m,\mu},m,r,\omega)\widetilde{p}_{G,m,2}(k^{\pm,S}_{m,\mu},r) \\ B^{\pm,S}_{m,\mu}(1)\widehat{q}^{\pm,S}_{G,m,2}(1)+\dfrac{\partial\widehat{q}^{\pm,S}_{G,m,2}}{\partial r}(1) = -\dfrac{\partial B^{\pm,S}_{m,\mu}}{\partial k}(1)p_{G,m,2}(k^{\pm,S}_{m,\mu},1) \\ \widehat{q}^{\pm,S}_{G,m,2}(1)=0, \end{cases} \quad \text{(B 6)}$$

noting that the order of the derivatives with respect to r and k can be switched. The right-hand sides of these equations are known for $k=k^{\pm,S}_{m,\mu}$ since $p_{G,m,2}$ and its radial derivative have previously been evaluated. As a result, the unknown function $\widehat{q}_{G,m,2}(k^{\pm,S}_{m\mu},r)$ is a solution of the second-order inhomogeneous linear differential equation (B 6) subject to the two boundary conditions on $r=1$. As previously, the problem is written as a system of two first-order equations

$$\frac{\mathrm{d}}{\mathrm{d}r}\mathbb{Z} = \mathbb{L}\mathbb{Z}+\mathbb{Z}_p, \quad \text{(B 7)}$$

with $\mathbb{L}$ defined by (B 2),

$$\mathbb{Z} = \begin{pmatrix} z_1 \\ z_2 \end{pmatrix} = \begin{pmatrix} r\widehat{q}^{\pm,S}_{G,m,2} \\ \dfrac{r}{D^{\pm,S}_{m,\mu}}\left(B^{\pm,S}_{m,\mu}\widehat{q}^{\pm,S}_{G,m,2}+\dfrac{\mathrm{d}\widehat{q}^{\pm,S}_{G,m,2}}{\mathrm{d}r}\right) \end{pmatrix}, \quad \text{(B 8)}$$

and $\mathbb{Z}_p$ is the inhomogeneous forcing

$$\mathbb{Z}_p = \begin{pmatrix} 0 \\ -\dfrac{r}{D^{\pm,S}_{m,\mu}}\left[\dfrac{\partial A}{\partial k}(k^{\pm,S}_{m,\mu},m,r,\omega)\dfrac{\partial\widehat{p}_{G,m,2}}{\partial r}(k^{\pm,S}_{m,\mu},r)+\dfrac{\partial B}{\partial k}(k^{\pm,S}_{m,\mu},m,r,\omega)\widehat{p}_{G,m,2}(k^{\pm,S}_{m,\mu},r)\right] \end{pmatrix}. \quad \text{(B 9)}$$

Equation (B 7) is solved by marching from $r=1$ to $r=h$ with the initial-value condition

$$\mathbb{Z}(1) = \left(0, \quad -\frac{1}{D^{\pm,S}_{m,\mu}(1)}\frac{\partial B^{\pm,S}_{m,\mu}(1)}{\partial k}p_{G,m,2}(1)\right). \quad \text{(B 10)}$$

Appendix C. Operators involved in (5.5) and (5.6)

We have

$$\mathscr{R}_{0,1}(\widetilde{G}) = \left[\frac{\partial}{\partial r_0}\left(\frac{\mathrm{D}_0}{\mathrm{D}t_0}\cdot\right) + \frac{\mathrm{d}(r_0U_\theta)}{r_0\,\mathrm{d}r_0}\frac{\partial}{r_0\,\partial\theta_0} + \frac{\mathrm{d}U_x}{\mathrm{d}r_0}\frac{\partial}{\partial x_0}\right]\mathscr{D}_0(\widetilde{G}) - 2\left[\frac{\mathrm{d}U_x}{\mathrm{d}r_0}\frac{\partial}{\partial x_0} + \frac{\mathrm{d}}{\mathrm{d}r_0}\left(\frac{U_\theta}{r_0}\right)\frac{\partial}{\partial\theta_0}\right]\frac{\mathrm{D}_0^2\widetilde{G}}{\mathrm{D}t_0^2} - \frac{\mathrm{d}}{\mathrm{d}r_0}\left[\frac{2U_\theta}{r_0^2}\frac{\mathrm{d}(r_0U_\theta)}{\mathrm{d}r_0}\right]\frac{\mathrm{D}_0\widetilde{G}}{\mathrm{D}t_0}, \quad (\mathrm{C}\,1)$$

$$\mathscr{R}_{0,2}(G) = U_\theta\mathscr{R}_{0,3}(G) + \frac{\mathrm{d}U_\theta}{\mathrm{d}r_0}\mathscr{R}_{0,4}(G) + \frac{\mathrm{d}U_x}{\mathrm{d}r_0}\mathscr{R}_{0,5}(G), \quad (\mathrm{C}\,2)$$

where

$$\mathscr{R}_{0,3}(G) = -\frac{8}{r_0^2}\frac{\mathrm{d}(r_0U_\theta)}{\mathrm{d}r_0}\frac{\mathrm{d}}{\mathrm{d}r_0}\left[\frac{U_\theta}{r_0^2}\frac{\mathrm{d}(r_0U_\theta)}{\mathrm{d}r_0}\right]G - \frac{2}{r_0^2}\frac{\mathrm{d}(r_0U_\theta)}{\mathrm{d}r_0}\frac{\partial}{\partial r_0}\left[\frac{\mathrm{D}_0^2G}{\mathrm{D}t_0^2}\right] - 4U_\theta\left[\frac{1}{r_0^2}\frac{\mathrm{d}(r_0U_\theta)}{\mathrm{d}r_0}\right]^2\frac{\partial G}{\partial r_0} + 4\frac{U_\theta}{r_0^4}\frac{\mathrm{d}(r_0U_\theta)}{\mathrm{d}r_0}\frac{\partial}{\partial\theta_0}\left[\frac{\mathrm{D}_0G}{\mathrm{D}t_0}\right], \quad (\mathrm{C}\,3)$$

$$\mathscr{R}_{0,4}(G) = \frac{2}{r_0}\frac{\partial}{\partial\theta_0}\left(\frac{\mathrm{D}_0^3G}{\mathrm{D}t_0^3}\right) \quad \text{and} \quad \mathscr{R}_{0,5}(G) = 2\frac{\partial}{\partial x_0}\left(\frac{\mathrm{D}_0^3G}{\mathrm{D}t_0^3}\right). \quad (\mathrm{C}\,4)$$

REFERENCES

ALI, A. A. & ATASSI, H. M. 2002 Scattering of acoustic and vorticity disturbances by an unloaded annular cascade in a swirling flow. In *8th AIAA/CEAS Aeroacoustics Conference and Exhibit, Breckenridge, CO*.

ATASSI, H. M., ALI, A. A., ATASSI, O. V. & VINOGRADOV, I. V. 2004 Scattering of incidence disturbances by an annular cascade in a swirling flow. *J. Fluid Mech.* **499**, 111–138.

BENDER, C. M. & ORSZAG, S. A. 1978 *Advanced Mathematical Methods for Scientists and Engineers. Asymptotic Methods and Perturbation Theory*. McGraw-Hill.

BERS, A. N. 1983 Space–time evolution of plasma instabilities – absolute and convective. In *Basic Plasma Physics, Handbook of Plasma Physics* (ed. A. A. Sudan & R. N. Galeev), vol. 1, pp. 451–517. North-Holland.

BRAMBLEY, E. J. 2007 The acoustics of curved and lined cylindrical ducts with mean flow. PhD thesis, University of Cambridge.

BRIGGS, R. J. 1964 *Electron-Stream Interaction with Plasmas*. MIT.

CARPENTER, P. W. 1985 A linearized theory for swirling supersonic jets and its application to shock-cell noise. *AIAA J.* **23**, 1902–1909.

CARPENTER, P. W. & JOHANNESEN, N. H. 1975 An extension of one-dimensional theory to inviscid swirling flow through choked nozzles. *Aeronaut. Q.* **26**, 71–87.

CHANAUD, R. C. 1965 Observations of oscillatory motion in certain swirling flows. *J. Fluid Mech.* **21**, 111–127.

COLONIUS, T. & LELE, S. K. 2004 Computational aeroacoustics: progress on nonlinear problems of sound generation. *Prog. Aeronaut. Sci.* **40**, 345–416.

COLONIUS, T., LELE, S. K. & MOIN, P. 1997 Sound generation in a mixing layer. *J. Fluid Mech.* **330**, 375–409.

COOPER, A. J. & PEAKE, N. 2002 The stability of a slowly diverging swirling jet. *J. Fluid Mech.* **473**, 389–411.

COOPER, A. J. & PEAKE, N. 2005 Upstream-radiated rotor–stator interaction noise in mean swirling flow. *J. Fluid Mech.* **523**, 219–250.

COOPER, A. J. & PEAKE, N. 2006 Rotor–stator interaction noise in swirling flow: stator sweep and leans effects. *AIAA J.* **44** (5), 981–991.

CURLE, N. 1955 The influence of solid boundaries upon aerodynamic sound. *Proc. R. Soc. Lond.* A **231**, 505–514.

DOAK, P. E. 1972 Analysis of internally generated sound in continuous materials: 2. A critical review of the conceptual adequacy and physical scope of existing theories of aerodynamic noise, with special reference to supersonic jet noise. *J. Sound Vib.* **25** (2), 263–335.

DOAK, P. E. 1973 Fundamentals of aerodynamic sound theory and flow duct acoustics. *J. Sound Vib.* **28** (3), 527–561.

DOWLING, A. P., FFOWCS WILLIAMS, J. E. & GOLDSTEIN, M. E. 1978 Sound production in a moving stream. *Proc. R. Soc. Lond.* A **288** (1353), 321–349.

ELHADIDI, B. & ATASSI, H. M. 2002 High frequency sound radiation from an annular cascade in swirling flows. In *8th AIAA/CEAS Aeroacoustics Conference and Exhibit, Breckenridge, CO*.

ELHADIDI, B. & ATASSI, H. M. 2003 High frequency formulation for interaction noise in annular cascades. In *9th AIAA/CEAS Aeroacoustics Conference and Exhibit*, Paper 2003-3133.

ELHADIDI, B., ATASSI, H. M., ENVIA, E. & PODBOY, G. G. 2000 Evolution of rotor wake in swirling flow. In *6th AIAA/CEAS Aeroacoustics Conference and Exhibit, Lahaina, HI.*

ENVIA, E., TWEEDT, D. L., WOODWARD, R. P., ELLIOTT, D. M., FITE, E. B., HUGHES, C. E., PODBOY, G. G. & SUTLIFF, D. L. 2008 An assessment of current fan noise prediction capability. In *14th AIAA/CEAS Aeroacoustics Conference and Exhibit, Vancouver, Canada*.

EVERS, I. & PEAKE, N. 2002 On sound generation by the interaction between turbulence and a cascade of airfoils with non-uniform mean flow. *J. Fluid Mech.* **463**, 25–52.

FARASSAT, F. 1977 Discontinuities in aerodynamics and aeroacoustics: the concept and applications of generalized derivatives. *J. Sound Vib.* **55** (2), 165–193.

FARASSAT, F. 1994 Introduction to generalized functions with applications in aerodynamics and aeroacoustics. *Tech. Rep.* Technical Paper 3428.

FFOWCS WILLIAMS, J. E. & HAWKINGS, D. L. 1969 Sound generation by turbulence and surfaces in arbitrary motion. *Proc. R. Soc. Lond.* A **264**, 321–342.

GLEGG, S. A. L. 1999 The response of a swept blade row to a three-dimensional gust. *J. Sound Vib.* **227** (1), 29–64.

GLEGG, S. A. L. & JOCHAULT, C. 1998 Broadband self-noise from a ducted fan. *AIAA J.* **36** (8), 1387–1395.

GOLDSTEIN, M. E. 1984 Aeroacoustics of turbulent shear flows. *Annu. Rev. Fluid. Mech.* **16**, 263–285.

GOLDSTEIN, M. E. 1976 *Aeroacoustics*. McGraw-Hill.

GOLDSTEIN, M. E. 2001 An exact form of Lilley's equation with a velocity quadrupole/temperature dipole source term. *J. Fluid Mech.* **443**, 231–236.

GOLDSTEIN, M. E. 2003 A generalized acoustic analogy. *J. Fluid Mech.* **488**, 315–333.

GOLDSTEIN, M. E., DITTMAR, J. H. & GELDER, T. F. 1974 Combined quadrupole–dipole model for inlet flow distortion noise from a subsonic fan. NASA Tech. Rep. TM D-7676.

GOLDSTEIN, M. E. & LEIB, S. J. 2008 The aeroacoustics of slowly diverging supersonic jets. *J. Fluid Mech.* **600**, 291–337.

GOLDSTEIN, M. E., SESCU, A. & AFSAR, M. Z. 2012 Effect of non-parallel mean flow on the Green's function for predicting the low frequency sound from turbulent air jets. *J. Fluid Mech.* **695**, 199–234.

GOLUBEV, V. V. & ATASSI, H. M. 1995 Aerodynamic and acoustic response of a blade row in unsteady swirling flow. In *1st AIAA/CEAS Aeroacoustics Conference and Exhibit, Munich, Germany*, vol. I, pp. 167–175.

GOLUBEV, V. V. & ATASSI, H. M. 1996 Sound propagation in an annular duct with mean potential swirling flow. *J. Sound Vib.* **198**, 601–616.

GOLUBEV, V. V. & ATASSI, H. M. 1998 Acoustic-vorticity waves in swirling flows. *J. Sound Vib.* **209**, 203–222.

GOLUBEV, V. V. & ATASSI, H. M. 2000*a* Unsteady swirling flows in annular cascades. Part 1. Evolution of incident disturbance. *AIAA J.* **38** (7), 1142–1149.

GOLUBEV, V. V. & ATASSI, H. M. 2000*b* Unsteady swirling flows in annular cascades. Part 2. Aerodynamic blade response incident disturbance. *AIAA J.* **38** (7), 1150–1158.

HANSON, D. B. 1976 Near field noise of high tip speed propellers in forward flight. In *3rd AIAA Aero-Acoustics Conference, Palo Alto, CA*.

HANSON, D. B. 2001*a* Broadband noise of fans. With unsteady coupling theory to account for rotor and stator reflection/transmission effects. Contractor Report CR-211136-REV1. NASA.

HANSON, D. B. 2001*b* Theory of broadband noise for rotor and stator cascade with inhomogeneous inflow turbulence including effects of lean and sweep. Contractor Report CR-210762. NASA.

HEATON, C. J. & PEAKE, N. 2005 Acoustic scattering in a duct with mean swirling flow. *J. Fluid Mech.* **540**, 189–220.

HEATON, C. J. & PEAKE, N. 2006 Algebraic and exponential instability of inviscid swirling flow. *J. Fluid Mech.* **565**, 279–318.

HOWE, M. S. & LIU, J. T. C. 1977 The generation of sound by vorticity waves in swirling duct flows. *J. Fluid Mech.* **81**, 369–383.

HUGHES, C. E., JERACKI, R. J., WOODWARD, R. P. & MILLER, C. J. 2002 Fan noise source diagnostic test – rotor alone aerodynamic performance results. In *8th AIAA/CEAS Aeroacoustics Conference and Exhibit, Breckenridge, CO*.

JONES, D. S. 1982 *The Theory of Generalised Functions*, 2nd edn. Cambridge University Press.

KARABASOV, S. A., AFSAR, M. Z., HYNES, T. P., DOWLING, A. P., MCMULLAN, W. A., POKORA, C. D., PAGE, G. J. & MCGUIRK, J. J. 2010 Jet noise – acoustic analogy informed by large eddy simulation. *AIAA J.* **48** (7), 1312–1324.

KERREBROCK, J. L. 1977 Small disturbances in turbomachine annuli with swirl. *AIAA J.* **15** (6), 794–803.

KHORRAMI, M. R. 1991 A Chebyshev spectral collocation method using a staggered grid for the stability of cylindrical flows. *Intl J. Numer. Meth. Fluids* **12**, 825–833.

KOCH, L. D. 2012 Predicting the inflow distortion tone noise of the NASA Glenn advanced noise control fan with a combined quadrupole–dipole model. In *18th AIAA/CEAS Aeroacoustics Conference and Exhibit, Colorado Springs, CO*.

KOUSEN, K. A. 1995 Eigenmode analysis of ducted flows with radially dependent axial and swirl components. In *1st AIAA/CEAS Aeroacoustics Conference and Exhibit, Munich, Germany*.

KOUSEN, K. A. 1996 Pressure modes in ducted flows with swirl. In *2nd AIAA/CEAS Aeroacoustics Conference and Exhibit*, Paper 96-1679.

LIGHTHILL, M. J. 1952 On sound generated aerodynamically: I. General theory. *Proc. R. Soc. Lond.* A **211** (1107), 564–587.

LILLEY, G. M. 1974 On the noise from jets. *AGARD CP-131*.

LLOYD, A. E. D. & PEAKE, N. 2008 Rotor–stator broadband noise prediction. In *14th AIAA/CEAS Aeroacoustics Conference and Exhibit, Vancouver, Canada*.

LU, H. Y., RAMSAY, J. W. & MILLER, D. L. 1976 Noise of swirling exhaust jets. In *3rd AIAA Aero-Acoustics Conference, Palo Alto, CA*.

MORFEY, C. L. 1971 Tone radiation from an isolated subsonic rotor. *J. Acoust. Soc. Am.* **49** (5), 1690–1692.

MORFEY, C. L. & WRIGHT, M. C. M. 2007 Extensions of Lighthill's acoustic analogy with application to computational aeroacoustics. *Proc. R. Soc. Lond.* A **463**, 2101–2127.

NAJAFI-YAZDI, A., BRÈS, G. A. & MONGEAU, L. 2011 An acoustic analogy formulation for moving sources in uniformly moving media. *Proc. R. Soc. Lond.* A **467**, 144–165.

NALLASAMY, M. & ENVIA, E. 2005 Computation of rotor wake turbulence noise. *J. Sound Vib.* **282**, 649–678.

NIJBOER, R. J. 2001 Eigenvalues and eigenfunctions of ducted swirling flows. In *7th AIAA/CEAS Aeroacoustics Conference and Exhibit, Maastricht, The Netherlands*.

PEAKE, N. & PARRY, A. B. 2012 Modern challenges facing turbomachinery aeroacoustics. *Annu. Rev. Fluid. Mech.* **44**, 227–248.

PODBOY, G. G., KRUPAR, M. J., HELLAND, S. M. & HUGHES, C. E. 2002*a* Steady and unsteady flow field measurements within a NASA 22 inch fan model. In *8th AIAA/CEAS Aeroacoustics Conference and Exhibit, Breckenridge, CO*.

PODBOY, G. G., KRUPAR, M. J., HUGHES, C. E. & WOODWARD, R. P. 2002*b* Fan noise source diagnostic test – LDV measured flow field results. In *8th AIAA/CEAS Aeroacoustics Conference and Exhibit, Breckenridge, CO*.

POSSON, H. 2008 Fonctions de réponse de grille d'aubes et effet d'écran pour le bruit à large bande des soufflantes. PhD thesis, Ecole Centrale de Lyon.

POSSON, H. & MOREAU, S. 2011 Rotor-shielding effect on fan-OGV broadband noise prediction. In *17th AIAA/CEAS Aeroacoustics Conference and Exhibit, Portland, OR*.

POSSON, H., MOREAU, S. & ROGER, M. 2010*a* On the use of a uniformly valid analytical cascade response function for broadband noise predictions. *J. Sound Vib.* **329** (18), 3721–3743.

POSSON, H., MOREAU, S. & ROGER, M. 2011 Broadband noise prediction of fan outlet guide vane using a cascade response function. *J. Sound Vib.* **330**, 6153–6183.

POSSON, H. & PEAKE, N. 2012 Acoustic analogy in swirling mean flow applied to predict rotor trailing-edge noise. In *18th AIAA/CEAS Aeroacoustics Conference and Exhibit, Colorado Springs, CO*.

POSSON, H. & ROGER, M. 2011 Experimental validation of a cascade response function for fan broadband noise predictions. *AIAA J.* **49** (9), 1907–1918.

POSSON, H., ROGER, M. & MOREAU, S. 2010*b* Upon a uniformly valid analytical rectilinear cascade response function. *J. Fluid Mech.* **663**, 22–52.

REINHARD, H. 1982*Equations Différentielles: Fondements et Applications*, chap. 6, pp. 257–279. Bordas.

RIENSTRA, S. W. 1999 Sound transmission in slowly varying circular and annular lined ducts with flow. *J. Fluid Mech.* **380**, 279–296.

ROGER, M. & ARBEY, H. 1985 Relation de dispersion des ondes de pression dans un écoulement tournant. *Acustica* **59**, 95–101.

TAM, C. K. W. & AURIAULT, L. 1998 The wave modes in ducted swirling flows. *J. Fluid Mech.* **371**, 1–20.

TOPOL, D. A. 1999 TFaNS tone fan noise design/prediction system. Volume I: System description, CUP3D technical documentation and manual for code developers. Contractor Report CR-1999-208882. NASA.

TYLER, J. M. & SOFRIN, T. G. 1962 Axial flow compressor noise studies. *SAE Trans.* **70**, 309–332.

VENTRES, C. S., THEOBALD, M. A. & MARK, W. D. 1982 Turbofan noise generation, Volume 1: Analysis. Contractor Report CR-167952. NASA.

YU, Y. K. & CHEN, R. H. 1997 A study of screech tone noise of supersonic swirling jets. *J. Sound Vib.* **205**, 698–705.